

1 **Nutrient and Carbon Export from a Tidewater Glacier to the Coastal Ocean in the Canadian Arctic**
2 **Archipelago**

3

4 **Patrick L. Williams^{1*}, David O. Burgess², Stephanie Waterman³, Megan Roberts⁴, Erin M.**
5 **Bertrand⁴, and Maya P. Bhatia^{1*}**

6 ¹ Department of Earth and Atmospheric Sciences, University of Alberta, Edmonton, AB, Canada

7 ² Geological Survey of Canada, Natural Resources Canada, Ottawa, ON

8 ³ Department of Earth, Ocean and Atmospheric Sciences, University of British Columbia,
9 Vancouver, BC, Canada

10 ⁴ Department of Biology, Dalhousie University, Halifax, NS, Canada

11

12 * Corresponding authors: Patrick Williams (plwillia@ualberta.ca) and Maya Bhatia
13 (mbhatia@ualberta.ca)

14

15 **Key Points:**

- 16 • Buoyant glacier meltwater plume entrains nutrient-rich deep water and delivers it to the
17 ocean surface at a shallow tidewater glacier
- 18 • Glacial meltwater directly contributes labile carbon to the ocean near the glacier terminus
- 19 • Higher concentrations of Chlorophyll *a* are associated with areas of glacier-driven
20 nutrient delivery

21 **Abstract**

22

23 As glaciers melt, a range of on-, in-, and under-glacier processes modify and export freshwater
24 and sediments to the ocean. This glacial runoff may influence biological productivity in coastal
25 ecosystems by supplying essential nutrients and labile carbon. Previous studies of glacial
26 meltwater export to the ocean have primarily been conducted on rivers draining land-terminating
27 glaciers, or in fjords with large tidewater glaciers. These studies speculate about downstream
28 effects (river studies) or upstream causes (fjord studies) of differing carbon and nutrient
29 availability and biological productivity, but do not measure them. Here, we conduct the first ice-
30 to-ocean study at a marine-terminating glacier in the Canadian Arctic Archipelago (CAA). We
31 characterize the nutrient and carbon content of ice and meltwater collected on the glacier surface,
32 at its margins, and in the near-shore coastal ocean, all within 1 to 25-km of the glacier terminus.
33 Results demonstrate that while meltwater from a shallow tidewater glacier did not directly
34 increase downstream carbon and nutrient concentrations, it can induce upwelling of deeper
35 nutrient-rich marine water. Also, although carbon concentrations in meltwater were low, results
36 show that this carbon is potentially more bioavailable than marine carbon. Glacially-mediated
37 delivery of labile carbon and upwelling of nutrient-rich water occurs in summer, when surface
38 waters are nutrient-limited. Collectively, these processes could benefit surface marine plankton,
39 potentially stimulating production at the base of the food web. Shallow tidewater glaciers are
40 commonly retreating in Arctic regions like the CAA and Svalbard, and understanding how
41 increased meltwater output from these systems impacts marine ecosystems is critical.

42 **Plain Language Summary**

43

44 As glaciers melt, nutrients and carbon contained in runoff may impact recipient marine
45 ecosystems. The last study to explore the relationship between tidewater glaciers and nutrient
46 availability in the Canadian Arctic Archipelago (CAA) was in the 1970s. Here we measure
47 nutrient and carbon concentrations in ice, glacial melt, and marine waters in front of a shallow
48 tidewater glacier in the CAA. We find that nutrient and carbon concentrations in glacial melt are
49 not high enough to augment downstream marine concentrations. However, the carbon in glacial
50 melt appears more protein-like and may be more bioavailable than marine carbon. Additionally,
51 with the release of submarine discharge at the terminal ice front, glacial meltwater entrains
52 deeper nutrient-rich marine water and delivers nutrients to the surface as the meltwater plume
53 rises. This upwelling is associated with the turbid meltwater plume and higher concentrations of
54 chlorophyll. Upwelling of nutrients forced by a shallow tidewater glacier, common in the
55 Canadian Arctic, could locally benefit surface marine plankton and stimulate production at the
56 base of the food web.

57 **1. Introduction**

58 Polar ice caps and glaciers in the Canadian Arctic Archipelago (CAA), Greenland and
59 Antarctica are melting faster than they were 30 years ago in response to climate change (Box et
60 al., 2018; Shepherd et al., 2020). Compared to the polar ice sheets, the CAA is populated by
61 smaller ice caps, icefields, and glaciers, and in the future, these ice masses may be particularly
62 susceptible to warming air temperatures (Cook et al., 2019). Similar to Greenland and
63 Antarctica, many ice caps and icefields in the CAA are drained by glaciers that terminate in the
64 ocean (Cook et al., 2019). Recent studies show that glacial runoff into the coastal ocean can
65 affect marine nutrient and carbon supply (Hawkings et al., 2015; Hood et al., 2009; Wadham et
66 al., 2016), coastal circulation (Straneo & Cenedese, 2015), and biological productivity (Juul-
67 Pedersen et al., 2015; Meire et al., 2017; Meire et al., 2015). Since most previous work
68 investigating glacially-mediated nutrient delivery has been undertaken on large tidewater glaciers
69 in Greenland, it is not clear whether the mechanisms by which large tidewater glaciers promote
70 marine productivity apply to the smaller ice masses present in the CAA (Hopwood et al., 2018).

71 Traditional knowledge from northern communities document waters off glacier termini to
72 be rich in wildlife (pers. comm. J. Qaapik, Grise Fiord Rangers). In 1938, “brown zones” in
73 waters adjacent to glaciers around Disko Bay (Greenland) were identified as areas of upwelling
74 that supported large populations of coastal birds (e.g. Kittiwake) which fed on zooplankton in a
75 freshened meltwater plume (Hartley & Dunbar, 1938). The ability of glaciers to erode and
76 deliver rock-derived nutrients like silicate (SiO_4^{4-}) and phosphate (PO_4^{3-}), important to
77 downstream phytoplankton communities, was also recognized early in the 20th century (Vibe,
78 1939). In the most recent study of glacially-derived nutrients in marine waters in the CAA,
79 Apollonio (1973) found elevated concentrations of nitrate (NO_3^-) and silicate within a glacierized
80 fjord when compared to a non-glacierized fjord before the spring thaw. Apollonio noted that
81 these nutrients were critical to arctic phytoplankton and augmented by glacial activity.

82 One main mechanism by which glacial melt can deliver nutrients and carbon to
83 downstream marine environments is via direct delivery of chemical constituents in meltwater. In
84 early summer, glacial runoff consists predominantly of surface snow melt which delivers a
85 source of atmospherically-deposited nitrate to the marine environment (Wolff, 2013). As the
86 melt season progresses, the proportion of ice melt in glacial runoff increases (Nienow et al.,

87 1998; Richards et al., 1996), which drains from the surface to the glacier bed via crevasses and
88 moulins (Boon & Sharp, 2003; Das et al., 2008). At the bed, glacial meltwater can become
89 chemically enriched in crustally-derived nutrients (e.g. silica, iron, and phosphorus) and carbon
90 (Bhatia et al., 2013b; Hawkings et al., 2016; Hawkings et al., 2017; Hood et al., 2009) before
91 discharging into the marine environment (Kanna et al., 2018). Numerous studies suggest that *in*
92 *situ* microbial communities on the glacier surface or at the bed are capable of high rates of
93 biogeochemical/physical weathering and cycling of organic carbon (Dubnick et al., 2017;
94 Dubnick et al., 2020). *In situ* microbial nitrogen fixation at the glacier bed is a second important
95 source of nitrate that may be delivered to marine waters (Boyd et al., 2011; Segawa et al., 2014;
96 Telling et al., 2012; Wadham et al., 2016). These communities can further provide labile protein-
97 like dissolved organic matter (DOM) to downstream environments (Bhatia et al., 2010; Hood et
98 al., 2009; Musilova et al., 2017). Over the course of the melt season, basal flow evolves from a
99 slow and distributed system, dominated by snow-melt and basal ice-melt, to a fast and
100 channelized one, dominated by ice-melt originating from the surface (Flowers, 2015; Gray,
101 2005; Hubbard et al., 1995). This evolution leads to shorter retention and rock-water interaction
102 times at the bed, and consequently lower entrained nutrient and carbon concentrations/fluxes
103 during peak melt (Brown, 2002; Sharp, 2005).

104 A second mechanism by which glacial melt can facilitate nutrient addition to coastal
105 waters is indirectly, via promoting the delivery of nutrients in deep nutrient-rich marine waters to
106 the near-surface by entrainment, upwelling, and mixing. At the terminus of tidewater glaciers,
107 runoff exits sub-glacially, sometimes hundreds of meters below the ocean surface (Straneo &
108 Cenedese, 2015). As the buoyant meltwater plume rises, it can entrain deep marine water
109 containing elevated levels of macronutrients (nitrate, phosphate, silicate) and transport it to the
110 surface. This entrainment of nutrient-rich deep water has been tied to locally high rates of
111 primary production observed in glacial fjords in Greenland and Svalbard (Halbach et al., 2019;
112 Kanna et al., 2018; Meire et al., 2017). Additionally, estuarine circulation in fjords fed by
113 glaciers can also drive upwelling and play an important role in nutrient delivery to the ocean
114 surface in areas influenced by freshwater (Etherington et al., 2007). The strong tidal currents and
115 shallow sill (moraine) entrances associated with glacial fjords and bays can further enhance
116 vertical mixing, which in turn can enhance the delivery of deep-water nutrients to the surface
117 (Etherington et al., 2007).

118 In the ocean, directly- or indirectly-sourced glacially-derived nutrients may fuel primary
119 autotrophic producers (phytoplankton) while labile carbon can feed microbial heterotrophs.
120 Phytoplankton communities require a host of macro- (e.g. nitrogen, phosphorus, silica) and
121 micro- (e.g. iron) nutrients to grow, but in the Arctic waters during the summer months, nitrogen
122 (N) is generally limiting following the spring bloom (Sorensen et al., 2017; Tremblay & Gagnon,
123 2009; Zhu et al., 2019). Since glacier meltwater delivery to the ocean occurs when NO_3^-
124 concentrations in surface waters are near zero, coastal phytoplankton communities could be
125 dependent on glacially-derived nutrients to sustain summer growth (Cape et al., 2018; Kanna et
126 al., 2018; Meire et al., 2017). In tandem, microbial heterotrophs may use glacially-derived
127 carbon, further stimulating higher trophic levels via the microbial loop (Azam & Malfatti, 2007).
128 Previous studies have found marine DOM to be recalcitrant, characterized by high humic-like
129 components, while glacial DOM tends to be more protein-like (bioavailable), suggesting that
130 glacially-derived carbon may better support downstream heterotrophic productivity (Bhatia et al.,
131 2013a; Hood et al., 2009; Musilova et al., 2017). The positive effects of glacial meltwater on the
132 availability of nutrients and carbon, and ultimately on productivity, are not necessarily restricted
133 to areas close to glacier termini, and they may extend further from shore to the continental shelf
134 (Cape et al., 2018; Painter et al., 2014).

135 Most previous work studying how glaciers impact marine nutrient and carbon availability
136 has been conducted either at land-terminating glaciers or in the ocean at large tidewater glaciers.
137 While some studies that span the ice-to-ocean continuum do exist (Halbach et al., 2019; Kanna et
138 al., 2018), there is a notable lack of research that considers the full ice-to-ocean system
139 (Hopwood et al., 2018; Meire et al., 2017). The absence of concurrent measurements on the ice
140 and in the ocean makes it challenging to determine whether enhanced nutrient concentrations
141 observed in coastal waters near tidewater glaciers (Kanna et al., 2018; Meire et al., 2017) are
142 controlled by direct delivery, deep water entrainment, or enhanced estuarine circulation.
143 Additionally, the regional focus on glacier systems in Greenland to date has led to a bias in the
144 modern literature towards large glaciers with deep submarine discharges draining into long fiords
145 at depths ≥ 140 meters below sea level (Cape et al., 2018; Kanna et al., 2018; Meire et al., 2017).
146 This bias may be problematic as according to these studies, the strength of meltwater-induced
147 upwelling, and thus the rate of indirect nutrient delivery, is largely dependent on the depth at
148 which submarine discharge enters the ocean and thus on the depth of the glacier grounding line

149 (Hopwood et al., 2018). Numerical models, based on these Greenland studies and parameterized
150 using deep outlet glacier systems (Hopwood et al., 2018; Oliver et al., 2020), propose a
151 productivity continuum between tidewater and land-terminating glaciers. These models predict
152 that as submarine discharge from tidewater glaciers becomes shallower, less nutrient-rich deep
153 water is delivered to the surface, and productivity enhancements decline as a result (Hopwood et
154 al., 2018). Further, these models indicate that if the glacier grounding line shoaled above a given
155 threshold depth (280 ± 200 m depth in the numerical model studied by Hopwood et al.), indirect
156 nutrient delivery becomes decoupled from the glacier meltwater flux, suggesting that deep and
157 shallow tidewater glaciers may impact indirect nutrient delivery to shallow waters in different
158 ways.

159 Very few measurements have been made at intermediate-depth (Meire et al., 2017) and
160 shallow-outlet (Halbach et al., 2019) tidewater glaciers. However, across the Arctic,
161 intermediate-depth and shallow-outlet tidewater glaciers are common. For example, in the Queen
162 Elizabeth Islands (northern CAA), the grounding line depth of tidewater glaciers averages ~ 230
163 m depth (Van Wychen et al., 2014) while on Baffin and Bylot Islands (southern CAA) grounding
164 lines are estimated to be ~ 100 m depth on average (Van Wychen et al., 2015). Similarly, in the
165 Svalbard archipelago, the average grounding line depth is estimated to be ~ 100 m depth
166 (Błaszczuk et al., 2009). These glacier systems are significantly shallower than typical tidewater
167 glaciers in Greenland, where the average grounding line depth is ~ 280 m depth (Morlighem et
168 al., 2017). Further, there is *in situ* evidence that shallow-outlet tidewater glaciers have the
169 potential to positively impact productivity: in a recent study of tidewater glaciers with grounding
170 lines of ≤ 70 m depth in Kongsfjorden, Svalbard, Halbach et al., (2019) reported the presence of
171 glacially-induced upwelling of nutrients in the fjord. Considering this result and the prevalence
172 of shallow-to-intermediate depth outlet tidewater glaciers across the Arctic, further observations
173 of shallow-terminating tidewater glaciers are necessary to gain a more complete understanding of
174 the impacts of melting glaciers on coastal biogeochemistry.

175 With the goal of determining how a shallow tidewater glacier impacts nutrient and carbon
176 availability in the proximate ocean, we conducted an ice-to-ocean study at Sverdrup Glacier,
177 Devon Island in the CAA. In contrast to many previous study sites, submarine discharge exits
178 Sverdrup Glacier relatively close to the surface. Here, we present *in situ* observations along a full
179 ice-to-ocean transect with observations extending from the glacier surface and margins upstream

180 of the glacier terminus, through the turbid subglacial discharge plume in the coastal ocean, to
181 more than 25 km out into open water (Jones Sound). Our study builds upon a very small number
182 of studies that have incorporated both on-ice and marine data to date (Halbach et al., 2019;
183 Kanna et al., 2018), and is the first in the CAA to document the biogeochemical influence of
184 glacial melt routed through the marginal and subglacial environments from ice to ocean.

185

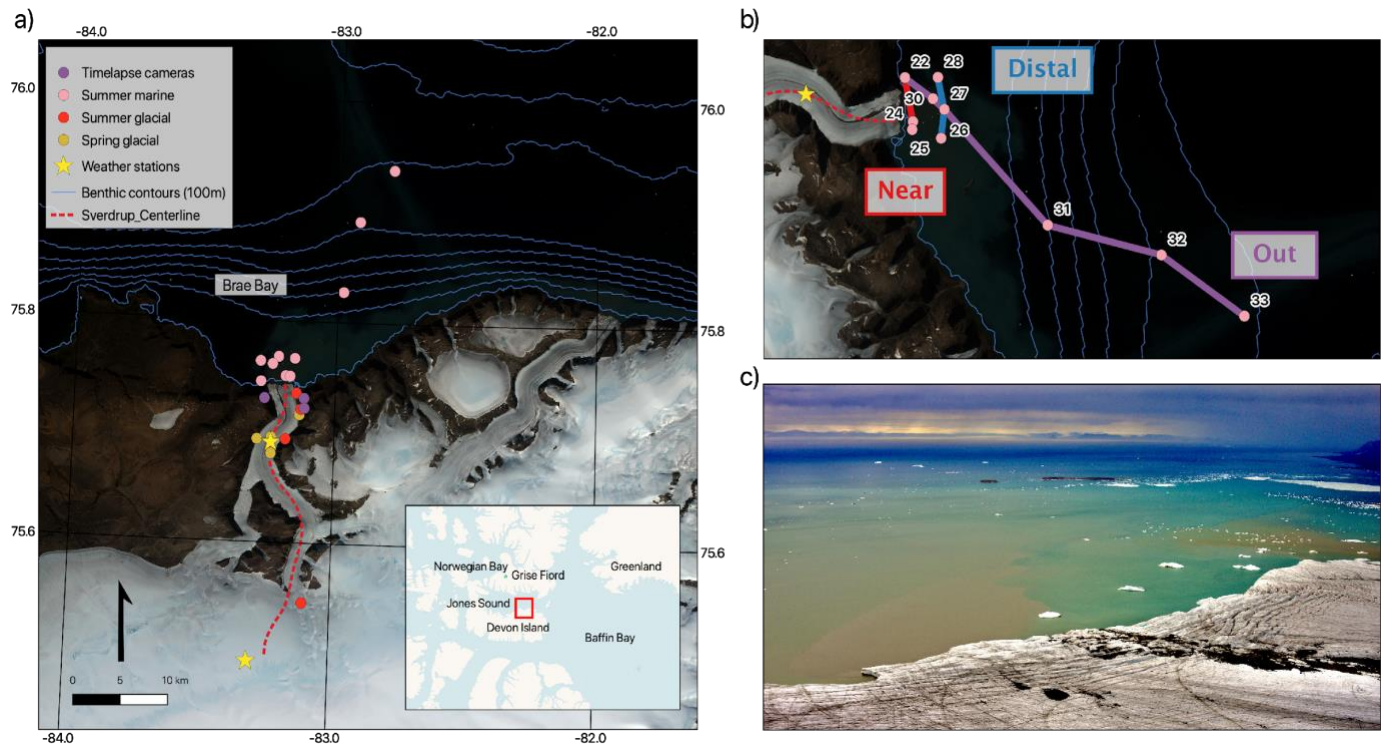
186 **2. Materials and Methods**

187 **2.1. Site Description**

188 *2.1.1 Sverdrup Glacier*

189 In 2019, spring (April 12 - May 12) and summer (July 22 - August 16) field sampling
190 campaigns were undertaken on Sverdrup Glacier, a polythermal marine-terminating glacier
191 located on the north coast of Devon Island, Nunavut Canada that drains ~805 km² (RGI
192 Consortium, 2017) of the northwest sector of Devon ice cap. The 25-km long warm-based
193 glacier overrides Precambrian metamorphic rocks of the Cumberland batholith, comprised
194 primarily of granulitic high-K to shoshonitic monzogranite and granodiorite, and small amounts
195 of low- and medium-K granitoid rocks (St-Onge et al., 2009; Whalen et al., 2010). Sverdrup
196 Glacier's north-south oriented valley is bordered by steep walls with an average height of 300 m
197 above the glacier surface (Vögtli, 1967). Surface mass balance and ice velocity measurements
198 were first made on Sverdrup Glacier in the 1960s (Koerner, 1970; Koerner et al., 1961; World
199 Glacier Monitoring, 2008), and six automatic weather stations (AWS) have been measuring air
200 temperature and changes in height of the ice/snow surface within the Sverdrup glacier basin
201 since 1999. The *in situ* measurements of ice velocity have shown that glacier flow rates typically
202 increase early in the melt season, an event first measured in 1961 (Cress & Wyness, 1961). This
203 seasonal acceleration points to a well-connected englacial/subglacial hydrological system driven
204 by inputs of supraglacial and ice-marginal meltwater draining to the glacier bed upstream from
205 the terminus (Wyatt & Sharp, 2017). Recent monitoring of Sverdrup glacier has shown larger
206 annual melt volumes associated with changes in climate. Surface mass balance (SMB) remained
207 only slightly negative up to the mid 1990's, then shifted to a period of increasingly negative

208 mass balance after 2005 when melt rates became ~4 times greater than the long-term average
209 (Sharp et al., 2011).



210

211 **Figure 1. Map of study site.** (a) Map of Sverdrup Glacier (Devon Island, Nunavut) showing
212 2019 spring on-ice (orange) and summer (red) sample sites, summer marine stations (pink), time
213 lapse camera locations (purple), weather stations (yellow stars), bathymetry (blue lines), and the
214 2012 IceBridge centerline (red dotted line). (b) Enlarged view of Brae Bay showing the three
215 “near” (red), “distal” (blue), and “out” (purple) transects used in this study. (c) View of the
216 terminus of Sverdrup Glacier on July 23, 2019 taken from the western terminus time-lapse
217 camera (orange circle outlined in pink) showing the turbid freshwater plumes at the glacier front.
218 Image brightness and contrast have been heightened for better plume visualization (see
219 Methods).

220

221 2.1.2 Marine Setting

222 Meltwater from Sverdrup Glacier discharges into a protected inlet, Brae Bay, Jones
223 Sound (Figure 1). The 5.12 km calving front is grounded on the seafloor (Dowdeswell et al.,
224 2004) with an annual calving flux of 0.006 Gt/y (Van Wychen et al., 2020). Based on a single
225 airborne radar sounding transect from the 2012 NASA Ice Bridge field program, (Paden et al.,
226 2019), ice within 1 km of the terminus is $\sim 20 \pm 10$ m thick (Sup. Figure 1). Unfortunately, the
227 location of this centreline thickness measurement (Figure 1, red dotted line) does not coincide

228 with that of the outflows of either of the submarine plumes observed in 2019. While much of the
229 surface meltwater runoff from Sverdrup Glacier is routed ice-marginally at higher elevations,
230 historical field observations, as well as those made in 2019, reveal that the bulk of marginal
231 meltwater enters the subglacial environment within 4 km of the glacier terminus (Keeler, 1964;
232 Koerner et al., 1961). Due to the relatively low ice flow velocities on Sverdrup glacier (Cress &
233 Wyness, 1961), fewer iceberg calving events have been observed here compared to other
234 tidewater glaciers draining the ice cap (Cress & Wyness, 1961; Dowdeswell et al., 2004). This
235 makes Sverdrup's terminus more readily accessible for oceanographic work than the termini of
236 more active glaciers.

237 Once released into the marine environment, meltwater enters Jones Sound, a waterway
238 between Devon Island and the southern end of Ellesmere Island. Water from the Arctic Ocean
239 enters Jones Sound via Cardigan and Hellgate to the west and from Nares Strait to the east.
240 Within Jones Sound, currents are cyclonic and the bulk of water exits the Sound into Baffin Bay
241 and ultimately the North Atlantic (Barber & Huyer, 1977; Melling et al., 2008; Zhang et al.,
242 2016). The bay in front of Sverdrup Glacier (Brae Bay) is hemmed by a series of submarine
243 moraines extending ~9 km off-shore from Sverdrup's existing terminus; these moraines are
244 located in shallow water, with some located less than 2 m below the surface (CHS Nautical Chart
245 7310, 2011).

246

247 **2.2. Field instruments and sampling**

248 *2.2.1 On-Ice Instrumentation and Sampling*

249 On-ice point measurements of surface mass balance were obtained from a network of 43
250 stakes drilled into the ice, and two automatic weather stations (AWS's) (Sup. Figure 1) in order
251 to validate spatially continuous gridded model data across the Sverdrup glacier basin. The mass
252 balance stake network spans the full elevational range from 100 to 1800 m a.s.l. including all
253 glaciological zones within the Sverdrup glacier basin. The upper AWS, i.e. DICS, used in this
254 study is situated at 1300m a.s.l., near the long-term equilibrium line altitude, while the lower
255 SVD station at 400 m a.s.l. is located in the ablation zone where the glacier surface thins by ~ 1
256 m annually due to summer melting. Air temperature and change in ice/snow surface height data

257 from these AWSs (Figure 2) provide high temporal (hourly) resolution for tracking the evolution
258 of the melt season; the latter are used to further assess bias in surface height modelling (see
259 Section 3.1).

260 Time-lapse cameras were deployed at three different locations on the glacier in April
261 2019 (Figure 1) to capture the seasonal evolution of surface and marginal melt and to constrain
262 characteristics of the freshwater plume that enters Jones Sound. These installations used Nikon
263 D-3200 cameras fitted with Nikkor 28 mm lenses to capture high-quality JPEG images. Cameras
264 were programmed to take an image every hour, provided there was enough light. The first photo
265 was taken on April 28, 2019 and images were downloaded on August 9, 2019. 271 photos were
266 taken by the time lapse cameras, but only images that were taken after the sea ice broke up and
267 were minimally impacted by cloud / fog were used (13 images total).

268 Spring samples from different glacier “end-member” freshwater sources (basal ice,
269 supraglacial snow / ice, and water stored at the base) were collected between April 23 and May
270 7, 2019. Bulk ice / snow / water samples were collected aseptically in trace metal clean ProPak®
271 bags (Teledyne ISCO) using an ethanol-rinsed and flame-sterilized steel chisel and aluminum ice
272 axe. Dissolved Organic Carbon (DOC) concentration and DOM fluorescence samples were
273 collected in pre-combusted amber glass EPA vials with PTFE-lined septa. DOC samples were
274 acidified with trace-metal grade concentrated HCl after collection to $\text{pH} \approx 2$. Samples were stored
275 frozen and in the dark until analysed in the laboratory.

276 Summer 2019 freshwater melt samples from supraglacial and marginal runoff streams
277 were collected between July 29 and August 15 and filtered in the field. Samples were collected
278 in cleaned and sterilized 2 L Teflon bottles. Nutrient and oxygen isotope samples were filtered
279 with sterile 60 mL plastic syringes, passed through a 0.22 μm polyethersulfone (PES) filter, and
280 stored in HDPE scintillation vials. Oxygen isotope samples were stored in the dark at ambient
281 temperature and nutrient samples were frozen within a few hours of collection. Samples for
282 DOC, Total Dissolved Nitrogen (TDN), and DOM fluorescence were filtered with all-plastic
283 polypropylene syringes (Norm-Jet), passed through a 0.22 μm PES filter, acidified to $\text{pH} \approx 2$
284 (DOC only) and stored in EPA vials as described above.

285

286 2.2.2 Marine Sampling

287 Ship-board work conducted from a polar sailboat (*S/Y Vagabond*) sampled the marine
288 waters in front of Sverdrup Glacier from August 4-8, 2019 (Figure 1). Sensor-based
289 hydrographic measurements, echo soundings, and bottle samples were taken at 12 marine
290 stations, of which 10 spanned three individual transects (“near”, “distal”, and “out”) in front of
291 the glacier terminus. Coordinates for all stations are provided in Sup. Table 1. Two lateral
292 transects, one termed “near” (located ~0.8 km from the ice terminus, stations 22, 24, and 25) and
293 the other “distal” (located ~2.5 km from the ice terminus, stations 26, 27, and 28), were sampled
294 to gain insight into how glacial melt altered the near-shore marine environment in Brae Bay. The
295 third transect (“out”, stations 22, 27, 30, 31, 32, and 33) followed the dispersion of a turbid
296 plume from within 1 km of the ice terminus to >25 km out into Jones Sound in order to track the
297 evolution in water column properties with increasing distance away from glacier terminus.

298 At each marine station, *in situ* measurements of electrical conductivity, temperature,
299 pressure, dissolved oxygen, photosynthetically active radiation, chlorophyll *a* (Chl *a*), and
300 turbidity were made using a RBRmaestro3 profiler (hereafter CTD). The CTD was hung from a
301 Dynema rope and at each station was allowed to equilibrate just below the surface. The CTD was
302 lowered by a winch at a rate of less than 1 m/s and recorded measurements at a frequency of 8
303 Hz. All data presented here were collected during the downcast.

304 Marine bottle sampling was also conducted at each station. Sample depths were chosen
305 using data collected during the CTD downcast and visualized in real-time with the Ruskin iOS
306 and Android app (RBR Ltd. 2017). At each station, multiple sample depths were selected: a near-
307 surface depth, the depth of the deep chlorophyll maximum (if present), and one or two deeper
308 sample depths (in the range of 50-400 m depth).

309 Marine water samples were collected using 10 L Teflon-lined, trace-metal-clean Go-Flo
310 bottles (General Oceanic) that had been soaked in 0.1% acid detergent (Citranox), rinsed 3x with
311 MilliQ, cleaned with isopropanol, soaked in 0.2 M HCl for 12 hours, and rinsed 3x with MilliQ
312 (Cutter & Bruland, 2012). Nutrient and oxygen isotope samples were collected directly from the
313 Go-Flo bottles with silicon tubing and filtered and stored as described above for the summer
314 freshwater samples, with nutrient samples immediately frozen after filtration. DOC, TDN, and
315 DOM fluorescence samples were also collected from the Go-Flo bottles into 2 L Teflon bottles,
316 and filtered, preserved and stored like the summer freshwater samples described above. Chl *a*

317 samples were collected in 4 L polycarbonate bottles, and between 600-1600 mL was vacuum-
318 filtered through a GF/F Whatman 47 mm filter in the dark, and then immediately frozen. All
319 plasticware, glassware, and tubing was soaked overnight in a 10% HCL bath and washed 3x with
320 MilliQ water. Glassware was then combusted at 560°C for ≥ 4 hours. All solvents used for
321 cleaning and sample analysis were trace-metal grade or better. In the field, plasticware and
322 glassware were rinsed 3x with sample water prior to collection.

323

324 **2.3. Laboratory analyses**

325 Prior to analysis, all frozen on-ice freshwater samples were thawed in a glass beaker in
326 the dark at 4 °C. Frozen marine samples were thawed in the dark at 4 °C in the original collection
327 bottles. Samples for nutrients (nitrate, nitrite, ammonia, phosphate, silicate), oxygen isotopes,
328 DOC, TDN, and DOM fluorescence properties were filtered through a glass vacuum apparatus
329 with 0.22 μm Teflon (PTFE) Omnipore filters into scintillation vials.

330 On-ice freshwater nutrient samples (nitrite, nitrate, phosphate, silicate, and ammonia)
331 were analyzed on a Lachat QuikChem 8500 series 2 flow injection analyzer at the Biological
332 Analytical Services Laboratory (University of Alberta), via photometric detection for
333 simultaneous measurement of nutrient concentrations. Samples and reagents were continuously
334 pumped through the system, loaded onto one or more injection valves, and mixed in the
335 QuikChem manifold under laminar flow conditions. Limits of detection (LODs) for
336 nitrite+nitrate, nitrite, ammonia, phosphate, and silica were: 0.15, 0.15, 0.21, 0.06, and 0.71 μM
337 respectively.

338 Marine nutrient samples (nitrite, nitrate, phosphate, silicate, and ammonia) were analyzed
339 on a Skalar SAN++ Continuous Flow Nutrient Analyzer at the Canada Excellence Research
340 Chairs Ocean Laboratory (Dalhousie University). Reagents and samples, segmented with air
341 bubbles, were pumped through a manifold for mixing and heating before entering the flow cell.
342 Nitrite, nitrate, phosphate, and silicate concentrations were detected colorimetrically with optical
343 background correction, while ammonia concentrations were determined with a fluorometer.
344 LODs for nitrite, nitrate, ammonia, phosphate, silicate were: 0.3, 0.15, 0.01, 0.2, and 0.08 μM
345 respectively.

346 DOC and TDN for both on-ice freshwater and marine samples were measured on a
347 Shimadzu TOC-V (CPH) analyzer. DOC was quantified as non-purgeable organic carbon
348 (NPOC) via high temperature combustion (680 °C) and TDN was measured with a total nitrogen
349 module. A 6-point standard curve was used with $R^2 \geq 0.9986$ and $R^2 \geq 0.9994$ for DOC and TDN
350 respectively. Standards were diluted from a 0.5 ppm stock solution for DOC (AccuSPEC, SCP
351 Science) and from potassium nitrate for TDN (Sigma, KNO_3) analyses. Reference standards for
352 deep seawater and low carbon water were obtained from the Consensus Reference Materials
353 Project (Hansell Laboratory, University of Miami). MilliQ blanks and reference waters were
354 analyzed routinely to monitor instrument drift, and remained within 5% of accepted values. The
355 LOD was 2.5 μM for DOC and 3.33 μM for TDN. Procedural blanks using MilliQ water filtered
356 through the plastic syringe and omnipore filters used in sample collection had DOC and TDN
357 concentrations below the detection limit.

358 The fluorescent characteristics of DOM were analyzed with a Horiba Aqualog-3
359 spectrofluorometer equipped with a xenon lamp. Samples were brought to room temperature
360 before analysis in a quartz glass cuvette with a 10 mm path length. Absorbance and excitation
361 scans were measured in 5 nm intervals from 230-600 nm with an integration time of 10 s with 10
362 nm slits. Emission spectra were measured from 218-618 nm with an excitation offset of 18 nm.
363 Ultrapure water in a dedicated cuvette (Mandel Scientific, SN-RM-H20) was used to validate the
364 instrument. Excitation emission matrices (EEMs) were corrected with a MilliQ blank using the
365 same settings.

366 Freshwater oxygen and deuterium isotopes were measured on a Picarro (L2140-i) at the
367 University of Alberta while isotopes in marine samples were measured on a Picarro (L2130-i) at
368 Dalhousie University. A volume of one μL of water was injected, vaporized, and introduced into
369 the analyzer and measurements of $\delta^{18}O$ and δD were obtained using cavity ring down
370 spectrometry. Certified water standards (USGS-46 and USGS-48) were used to normalize raw
371 isotope ratios to the Vienna Standard Mean Ocean Water-Standard Light Antarctic Precipitation
372 (VSMOW-SLAP) scale. For both instruments, analytical error was $<0.5\%$ for δD and
373 $<0.15\%$ for $\delta^{18}O$ (one standard deviation) based on routine analysis of an internal deionized
374 water standard (QCDI 6-2).

375 Chl *a* was measured using a Turner Designs AquaFluor Handheld Fluorometer following
376 EPA Method 445 (Arar & Collins, 1997). Whatman 47 mm GF/F filters were extracted in 10 mL
377 of 90% acetone for 18-24 hours. A 5 mL aliquot of the supernatant was transferred to a glass
378 cuvette and the fluorescence was measured. Samples were then acidified to 0.003 N using 0.1 N
379 HCl and fluorescence was measured again to account for interference from non-photosynthetic
380 phaeopigments. The fluorometer was calibrated using a pure Chl *a* standard (C5753, Sigma). The
381 LOD for Chl *a* analysis was 0.024 ug/L of seawater.

382

383 **2.4. Data processing and analyses**

384 *2.4.1 Plume detection from time-lapse images*

385 A k-means pixel classification was performed on a subset of the images from the time-
386 lapse camera (13 images total) following Danielson and Sharp (2017) to detect the extent of the
387 plume exiting Sverdrup's terminus. To minimize the effects of the sun's reflection, only images
388 taken between 22:00 and 04:00 UTC were used. Land and sky were masked before pixel
389 classification commenced. The k-means algorithm allowed for color-based plume detection at
390 Sverdrup's terminus in a variety of light conditions. The process followed four steps: 1) data
391 cleaning, filtering, and color-correction; 2) k-means classification; 3) pixel area to relative area
392 conversion; and 4) comparison of plume area over time. The k-means pixel classification was
393 conducted in R following the algorithms described in (MacKay, 2003). Ten clusters were used in
394 the analysis. While the clustering analysis detected the plume, the calculated color was not
395 consistent across images and was therefore selected manually for each image. Converting pixel
396 areas to relative areas was also done in R using a monophotogrammetric technique from
397 Krimmel and Rasmussen (1986).

398

399 *2.4.2 CTD data processing*

400 Raw CTD data were processed using the Matlab *rsktools* toolbox distributed by RBR Ltd.
401 Measured conductivity, temperature, and water pressure were used to derive salinity, depth, and
402 seawater density according to the 2010 thermodynamic equation of seawater (McDougal &
403 Barker, 2011). Salinity, depth, dissolved oxygen, PAR, Chl *a*, and turbidity vertical profiles were

404 built by applying a low-pass filter to match sensor time constants using a three-sample running
405 average, and channels were binned by pressure into 1-m intervals for further analysis. The
406 euphotic zone depth, defined as the depth at which PAR=0.1% of the surface value (see Banse,
407 2004), was also calculated at each station using CTD measurements of PAR.

408

409 *2.4.3 Optical properties of DOM*

410 Parallel Factor Analysis (PARAFAC) is a statistical tool used to decompose trilinear data
411 arrays to identify and quantify independent underlying signals or “components” (Bro, 1997).
412 This technique can be applied to EEMs (excitation/emission matrices - a three-order array of
413 sample name, excitation wavelength, and emission wavelength) to break down complex spectra
414 into generalized DOM components (Stedmon & Markager, 2005). While these components
415 cannot be ascribed to specific organic species, they can be compared to previously described
416 DOM fractions. The drEEM toolbox in Matlab (Murphy et al., 2013) was used to model five
417 individual fluorescent components. Corrections for instrument spectral bias and inner filter
418 effects were applied and Raman scatter was normalized using daily scans. EEMs were smoothed
419 and normalized to unit variance. PARAFAC models were validated using split-half analysis
420 (Murphy et al., 2013), making sure that each split dataset contained a mix of fresh and marine
421 samples. Modeled components were compared to previous glacial studies (Dubnick et al., 2017;
422 Fellman et al., 2010a; Fellman et al., 2010b; Hood et al., 2009; Pautler et al., 2012; Walker et al.,
423 2009) and other published models in the OpenFluor database (Murphy et al., 2014). To
424 summarize optical DOM composition across samples, fluorescent intensity of each component
425 was summed and normalized. Principal component analysis (PCA), analysis of variance
426 (ANOVA), and permutational multivariate analysis of variance (PERMANOVA) were
427 subsequently performed in *R* using the *vegan* package.

428

429 *2.4.4 Apparent oxygen utilization calculations*

430 Apparent oxygen utilization (AOU) is the difference between measured dissolved O₂ and
431 the theoretical equilibrium saturation concentration in water with the same physical and chemical
432 properties. Differences between measured and theoretical dissolved O₂ concentrations are

433 usually a result of biological activity: elevated primary production increases dissolved oxygen
434 concentration, while respiration consumes oxygen and decreases dissolved oxygen
435 concentration. Thus, AOU can be a measure of the sum of all biological activity a sample has
436 undergone since its last contact with the surface (Garcia et al., 2013). AOU was calculated using
437 measured temperature, dissolved oxygen, and salinity as per Benson and Krause (1984) with the
438 *LakeMetabolizer* toolbox in R.

439

440 2.4.5 Statistical analyses

441 All further statistical analyses were conducted in R using the *akima*, *candisc*, *caret*,
442 *cowplot*, *ecodist*, *ggbiplot*, *ggisoband*, *interp*, *klaR*, *MASS*, *MBA*, *NISTunits*, *oce*, *ocedata*,
443 *openair*, *gdal*, *RVAideMemoire*, and *zoo* packages.

444

445 2.5 Glacier surface mass balance modeling

446 Finally, in order to better constrain the meltwater inputs to the marine system we
447 modelled the surface mass balance of the Sverdrup Glacier basin for the time period spanning
448 our on-ice and marine observations. To do this, we estimate total meltwater runoff for the
449 Sverdrup glacier basin (as defined by the Randolph Glacier Inventory v6 RGI Consortium, 2017;
450 Table S1) from the 1 km resolution RACMO2.3 regional climate model (Noël et al., 2018) over
451 the 2019 melt season as:

$$452 \quad MF = \sum_{k=1}^{days} \sum_{j=1}^{Nsb} Sb$$

453 where MF is the meltwater flux, $days$ is the number of days since Julian day (JD) 182 (July 1st),
454 Nsb is the number of daily RACMO2.3 grid cells showing negative balance, and Sb is the value
455 of each 1 x 1 km grid cell. Values of MF were converted from centimeters to kilometers to
456 provide a measure in gigatons of total melt. We assume that all melt is routed to the tidewater
457 terminus where it enters the ocean. As such, retention of meltwater within the remaining
458 snowpack and / or firn is not accounted for in this study.

459 Independent validation of model performance over the Sverdrup glacier basin was
460 performed by comparing spatially-coincident 1 km grid cells with *in situ* measurements of SMB
461 as per Burgess (2018). Comparisons of cumulative SMB from RACMO2.3 with *in situ*
462 measurements at each AWS (1 km resolution) provided daily validation of the intensity and
463 duration of melt over the summer of 2019 as estimated from RACMO2.3 (Sup. Figure 2b and
464 2c). Results from these comparisons show that between measured and modeled SMB,
465 RACMO2.3 results over-estimated summer melt by 20.4 mm w.e. at the SVD AWS and by 124
466 mm w.e. at the DICS AWS. It should be noted that the AWSs record single point measurements
467 of ablation, while the RACMO2.3 data are averaged over 1km²; as such, some discrepancy
468 between measured and modelled values is expected. While both AWSs are situated in fairly
469 different settings, i.e. DICS is exposed to high winds on the ice cap proper and the SVD station
470 is relatively sheltered from the wind by the surrounding mountains in the Sverdrup glacier
471 valley, both sites are situated on very shallow slopes (<1°). AWS locations are also both
472 characterised by relatively low relief (< 0.5 m) sastrugi (wave-like features in snow caused by
473 wind erosion) during the winter months. A higher degree of spatial variability occurs at SVD
474 station during the summer months where surface ponds, stream channels and cryoconites are
475 more common than at the higher elevation DICS. Reduced albedo due to the presence of these
476 features could account for the bias towards higher estimations of modelled melt than was
477 measured at the SVD station. Uncertainty of the total melt discharge from the Sverdrup glacier
478 basin in 2019 as modelled by RACMO2.3 was assessed through comparisons with
479 melt/accumulation measured at each stake in the Sverdrup glacier basin over the period from
480 2008 to 2015. The standard deviation of the differences between RACMO2.3 and *in situ*
481 measurements averaged for all stakes indicate an uncertainty of ±120 mm w.e., with better
482 agreement (±90 mm w.e.) at higher elevations (≥1200m a.s.l.) than at lower elevations (±110 mm
483 w.e. at ≤400 m a.s.l.). This standard deviation corresponds to an uncertainty of ±0.1 Gt (Sup.
484 Figure 2a) in modelled estimates of total meltwater flux from the Sverdrup glacier basin.

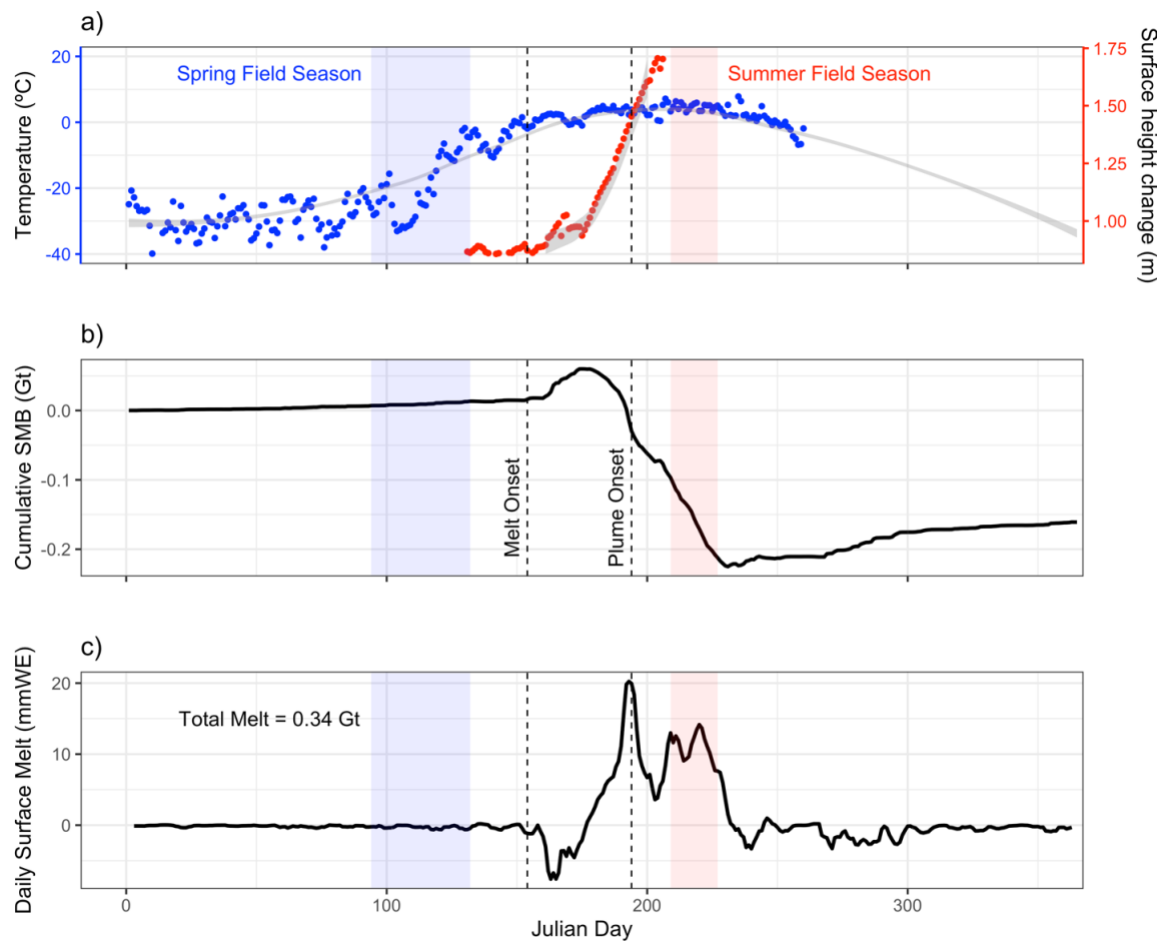
485

486 **3. Results**

487 **3.1. Meltwater export**

488 AWS and RACMO2.3 SMB data provide context for the timing and volume of meltwater
489 exported from Sverdrup in 2019. AWS data confirms that the spring season glacial samples were
490 collected pre-melt (Julian Days 94-132, Figure 2 blue box) and that summer season samples
491 were collected during peak melt (Julian Days 209-227, Figure 2 red box). The net SMB directly
492 measured at both AWSs and at 43 ablation stakes from 2008-2015 are consistent with previous
493 work comparing RACMO2.3 results to SMB in the CAA (Burgess, 2018) and are in agreement
494 with past assessments of RACMO2.3 SMB, where errors between measured and modeled melt
495 were generally good ($\pm 4\%$), except for terminus regions on Agassiz, Devon, and Penny ice caps
496 in the CAA (Noël et al., 2018). RACMO2.3 data from 2018-2019 for the Sverdrup watershed
497 shows 0.34 Gt of summer melt over a 55 day melt season (Figure 2c). The first sign of summer
498 melt (JD 154) was followed by ~ 10 days of net accumulation, with daily melt volumes peaking
499 when the plume was first observed (Figure 2b). Summer field sampling took place during the
500 second highest period of daily surface melt, and as sampling took place toward the end of the
501 melt season, cumulative surface melt was near its highest.

502 The time-lapse camera (TLC) imagery and field observations at Sverdrup's terminus
503 provide an independent and complementary characterization of the seasonal timing and
504 characteristics of the turbid meltwater plume released at the ice front in 2019. These images and
505 observations showed two persistent patches of turbid water in front of the terminus, one smaller
506 and one larger, which were interpreted as the signatures of freshwater subglacial plumes rising to
507 the surface. The main plume appeared to be discharged on the western side of the glacier, while a
508 smaller plume was evident on the eastern side. TLC images showed that the first signs of
509 summer melt (Julian Day 154, Figure 2b blue box) and plume development (Julian Day 194
510 Figure 2b red box) occurred on June 3 and July 13 (2019), respectively. Sup. Figure 3 shows
511 results of the k-means pixel classification and an example image from the data set. Detected
512 plume area was correlated with modeled cumulative surface mass balance (i.e. plume area
513 increased as Sverdrup glacier lost mass over the melt season) from the AWS ($r=-0.71$, $p=0.015$,
514 Sup. Figure 3c). This correlation gives confidence that detecting plume areas using this method
515 is reasonable.



516

517 **Figure 2. Sverdrup mass balance summary.** (a) Temperature (blue) and surface height change
 518 (red) data from SVD AWS. Gray fill represents the 95% confidence interval of 2016–2018
 519 temperature and surface height change AWS measurements. (b) Daily and (c) cumulative 2019
 520 RACMO2.3 surface mass balance data for Sverdrup Glacier. Melt and plume onset dates
 521 determined using time lapse camera imagery (black dotted lines) and the duration of the spring
 522 and summer 2019 sampling periods (blue and red shading) are shown in all panels.

523

524 3.2. Meltwater nutrient delivery

525 Analyses of on-ice and marine bottle samples for nutrient concentrations gives insight
 526 into the role of glacial discharge in the direct delivery of chemical species to the marine
 527 environment. Table 1 shows a summary of macronutrient (NO_3^- , PO_4^{3-} , SiO_4^{4-} , NH_4^+) and TDN
 528 concentrations for glacial and marine samples. Marine samples are summarized for both the
 529 upper (≤ 40 -m depth) and deep (> 40 -m depth) water column in both relatively close proximity to
 530 the glacier front (≤ 4 km) and beyond 10 km from the glacier terminus. “Spring Glacial” samples

531 represent a variety of glacial environments (i.e., basal ice, supraglacial snow, supraglacial ice,
532 and overwinter water) while “Summer Glacial” samples consist of marginal runoff and supra-
533 and subglacial melt. Geochemically, spring glacial samples had higher macronutrient
534 concentrations and fluxes compared to summer glacial samples, indicating that the export of
535 macronutrients to the marine environment may have significant seasonal variability. In contrast,
536 DON did not vary significantly with season. The lower concentrations of macronutrients in
537 summer glacial samples likely reflect shorter retention and rock-water interaction times and the
538 absence of snow in late-season melt (Nienow et al., 1998; Richards et al., 1996; Wolff, 2013). A
539 higher degree of variability in spring relative to summer glacial samples likely reflects the
540 diversity of sample types collected. Concentrations of macronutrients, except for ammonia, were
541 all lower in glacial samples compared to deeper marine (>40-m depth) samples.

542

543

544 **Table 1. Glacial freshwater and marine seawater values.** Average and standard deviations for
 545 biogeochemical parameters (BLD = below limit of detection). Average values are given for
 546 marine depths as indicated. Samples ≤ 4 km from Sverdrup's terminus are within the moraines
 547 surrounding Brae Bay. The number of samples (n), is also given.

548

Sample Type	n	NO ₃ ⁻ (μ M)	PO ₄ ³⁻ (μ M)	SiO ₄ ⁴⁻ (μ M)	NH ₄ ⁺ (μ M)	TDN (μ M)	$\delta^{18}\text{O}$ (‰)	DOC (μ M)	Chl a (μ g/L)
Spring Glacial	10	2.2 \pm 0.3	0.3 \pm 0.0	5.0 \pm 0.2	1.4 \pm 0.1	1.8 \pm 0.2	-27.8 \pm 0.4	16.4 \pm 1.1	---
Summer Glacial	11	1.8 \pm 0.0	0.1 \pm 0.0	*BDL	1.2 \pm 0.0	1.8 \pm 0.0	-26.7 \pm 0.2	10.9 \pm 0.4	---
Marine ($\leq 40\text{m}, \leq 4\text{km}$)	18	2.0 \pm 1.8	0.5 \pm 0.2	5.6 \pm 3.4	1.5 \pm 1.8	5.6 \pm 2.8	-3.0 \pm 1.0	63.9 \pm 44.2	2.2 \pm 2.4
Marine ($\leq 40\text{m}, >10\text{km}$)	6	1.4 \pm 2.2	0.5 \pm 0.3	4.2 \pm 4.2	0.9 \pm 0.5	5.8 \pm 2.4	-2.0 \pm 0.2	97.7 \pm 40.8	1.6 \pm 1.5
Marine ($>40\text{m}, \leq 4\text{km}$)	3	6.6 \pm 0.2	0.9 \pm 0.1	12.9 \pm 0.3	0.3 \pm 0.5	12.2 \pm 1.2	-1.7 \pm 0.0	126.9 \pm 20.7	0.1 \pm 0.1
Marine ($>40\text{m}, >10\text{km}$)	7	6.5 \pm 3.1	0.7 \pm 0.1	11.1 \pm 3.4	1.8 \pm 1.2	10.5 \pm 5.9	-1.3 \pm 0.7	78.6 \pm 26.6	0.4 \pm 0.5

549

550 **3.3. Meltwater carbon delivery**

551 In addition to the potential for delivering nutrients, glacial discharge may also impact
 552 downstream carbon availability via the delivery of DOC in meltwater. Average and standard
 553 deviation DOC concentrations in spring and summer glacial samples as well as marine samples
 554 are shown in Table 1. Similar to macronutrient concentrations, there was more variability in
 555 DOC concentrations in spring glacial samples compared to summer samples, likely representing
 556 the larger variety of different sample types collected during the spring season. Further, also as
 557 with macronutrient concentrations, DOC concentrations in meltwater in both seasons were
 558 universally lower than marine concentrations. Given this, it appears that Sverdrup glacier does
 559 not export DOC in concentrations high enough to significantly augment DOC concentrations in
 560 the marine environment.

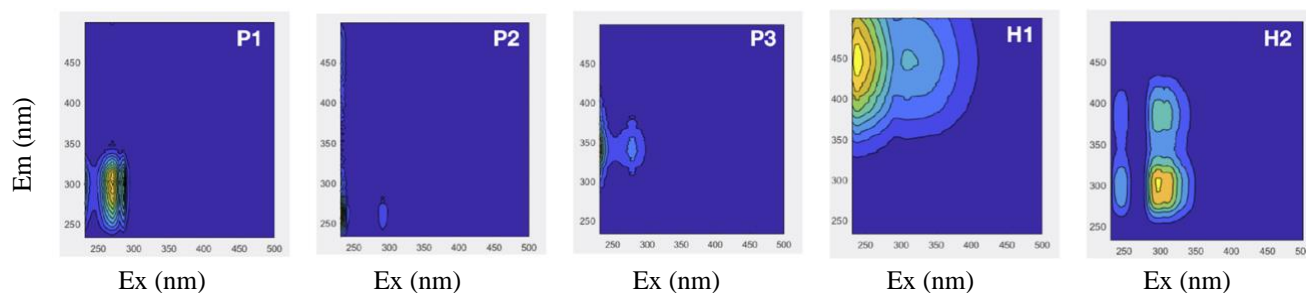
561 Though spring and summer glacial DOC concentrations were lower than those in marine
 562 samples, PARAFAC results show that the type of carbon present in spring and summer glacial
 563 water was significantly different than in marine waters; we thus explored the generalized DOM

564 component composition of glacial and marine samples to gain insight into the possible influence
565 of glacial input on DOM in the near-shore marine environment. A five-component PARAFAC
566 model applied to all spring glacial, summer glacial, and marine samples explains 97.7% of the
567 variance in the dataset. The loading patterns of the five modeled components can be matched to
568 previously-described fluorescent DOM fingerprints in glacierized environments (Table 2). P1
569 (tyrosine) and P2 (tryptophan) match protein-like peaks identified in marine and terrestrial
570 samples from around the world (Coble, 1996) and broadly indicate autochthonous production of
571 DOM (Stedmon & Markager, 2005). P3 has been found in glacial ice and meltwaters from the
572 McMurdo Dry Valleys (Antarctica) as well as on Axel Heiberg and Ellesmere Islands in the
573 CAA (Dubnick et al., 2017; Pautler et al., 2012). Components H1 and H2 are similar to
574 previously described humic-like peaks. H1 is similar to a humic-like component of terrestrial
575 origin ubiquitous to a wide range of natural catchments during the warmer months of the year
576 and generally absent in wastewater (Stedmon et al., 2007). H2 is similar to the classic M peak
577 (Coble, 1996) and has been defined as a marine humic-like component. Respectively, spring and
578 summer glacial samples contained >40% and ~18% more protein-like components than marine
579 samples. In contrast, marine samples had >60% more humic-like DOM compared to summer
580 glacial samples and >300% more humic-like DOM relative to spring glacial samples. Though
581 bulk DOM concentrations in glacial melt were not high enough to significantly increase marine
582 concentrations, proportionally, there was significantly more protein-like DOM in glacial melt vs.
583 in marine waters, with more protein-like DOM in spring glacial melt compared to summer
584 meltwater. There was also a higher fraction of the P1 component (associated with summer
585 glacial melt) in the higher turbidity marine samples compared to marine samples outside the
586 turbid meltwater plume. It thus appears that the freshened and turbid submarine meltwater plume
587 delivers protein-like DOM to the surface of Brae Bay with a carbon signature similar to summer
588 meltwater. This may be significant because secondary producers (marine heterotrophs) could
589 benefit from this addition of bioavailable carbon.

590

591

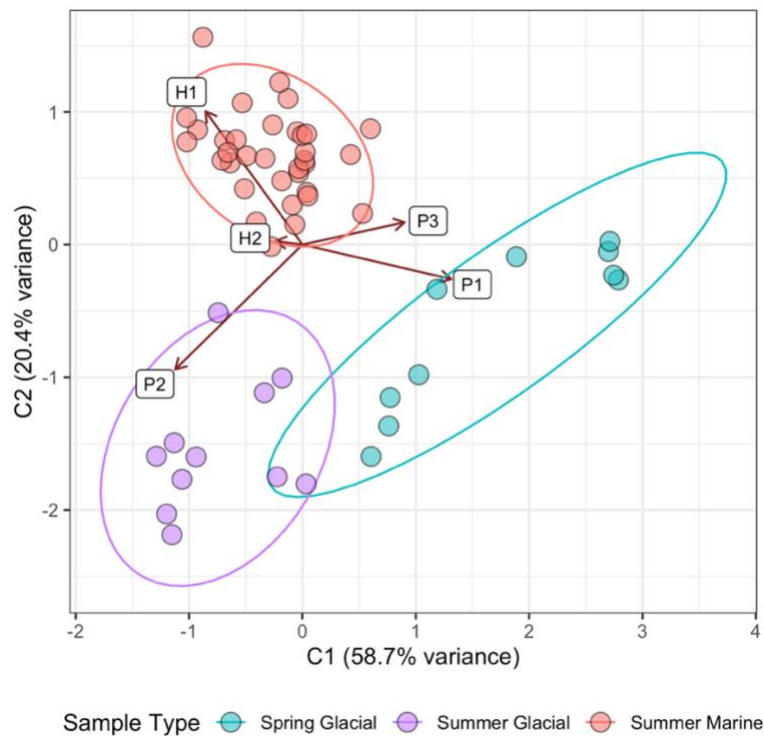
592 **Table 2. A summary of the 5 PARAFAC components.** Components modeled using fresh and
 593 marine samples from Sverdrup Glacier and Brae Bay (n = 55). Described here are wavelengths
 594 (nm) of the component excitation (Ex) and emission (Em) spectral peaks, the potential carbon
 595 source (protein-like vs. humic-like), and examples of previous studies that have found similar
 596 peaks in similar environments.



Component	Ex:Em (nm)	Potential Carbon Source	Literature Examples
P1	270: 301	Protein-like (Tyrosine)	Stedmon, 2005; Walker, 2009; Fellman, 2010
P2	290: 265	Protein-like (Tryptophan)	Coble, 1996; Walker, 2009; Fellman, 2010
P3	280: 337	Protein-like (autochthonous DOM via microbial degradation)	Coble, 2007; Pautler, 2012; Dubnick, 2010
H1	235, 310:441	Ubiquitous humic-like	Stedman, 2005; Stedmon, 2007; Dubnick, 2010
H2	245, 295:300, 395	Marine humic-like (microbial degradation)	Coble, 1996; Walker, 2009

597

598 To further assess seasonal and spatial differences in fluorescent DOM composition, a
 599 principal component analysis (PCA) was conducted using the relative abundance of the 5
 600 modeled PARAFAC components (Figure 3). The first and second principal components
 601 described 58.7% and 20.4% of the variance in the normalized PARAFAC dataset, respectively.
 602 PCA results show a clear differentiation between glacial and marine samples and between the
 603 spring and summer glacial samples. A PERMANOVA test confirms that these clusters are
 604 significantly different ($p < 0.004$) while the ANOVA f-test ($f > 10^{20}$) confirms that this difference
 605 is due to between-group variability. P1 and P3 are associated with spring melt, P2 is associated
 606 with summer melt, and H1 and H2 are associated with summer marine samples. This analysis
 607 confirms the unique DOM signatures of the glacier meltwater relative to the marine waters, and
 608 further the seasonal evolution of meltwater DOM characteristics.



610

611 **Figure 3. Principal component analysis (PCA) of the five modeled PARAFAC components.**
 612 Data is grouped by season (spring vs. summer) and water type (glacial vs. marine). A
 613 PERMANOVA test ($p < 0.004$) confirms these clusters are significant while the ANOVA f-test (f
 614 > 1020) confirms that this significance is due to between-group variability.

615

616 3.4. Glacial meltwater in the near-shore marine environment

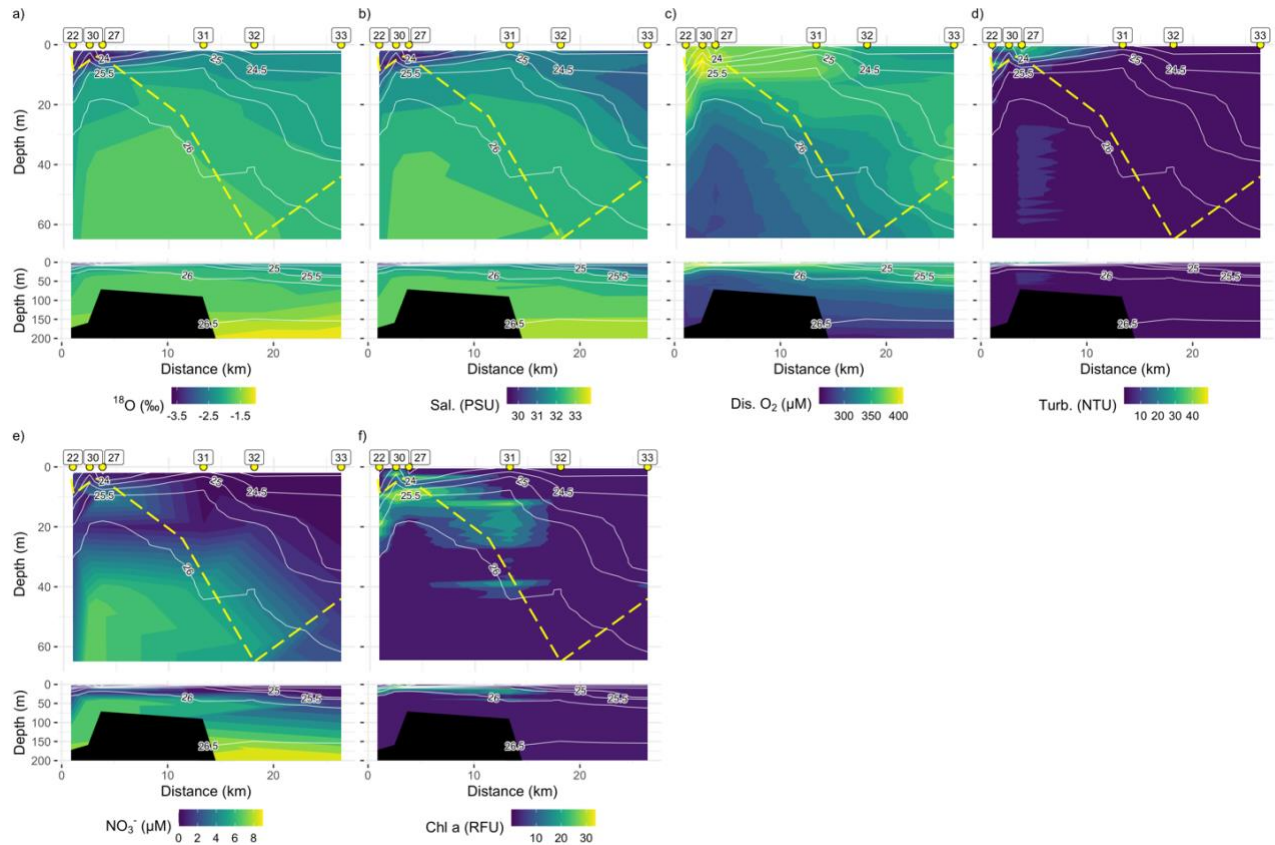
617 The fate of glacial meltwater in the marine environment is mapped by measurements of
 618 $\delta^{18}\text{O}$, salinity, oxygen, and turbidity in marine water sampled at various locations relative to the
 619 glacier terminus. Specifically, marine profiles along the “near” (~0.8 km from the ice terminus),
 620 “distal” (~2.5 km from the ice terminus), and “out” (from within 1-km to more than 25 km from
 621 the ice terminus) transects suggests that glacial meltwater is largely confined to the upper 30-40
 622 m of the water column, directly impacting waters ≤ 4 km from the glacier front. Marine water
 623 column profiles show a spatial gradient in $\delta^{18}\text{O}$ (Figure 4a), salinity (Figure 4b), dissolved
 624 oxygen (Figure 4c), and turbidity (Figure 4d), with fresher, more ^{18}O -depleted, oxygen-rich, and
 625 turbid waters found closer to the ocean surface and the calving front. ^{18}O -depleted water is

626 characteristic of glacial meltwater due to Rayleigh fractionation (Tranter, 2011). The “out”
627 transect (Figure 4) shows a clear spatial correlation between ^{18}O -depletion (glacial melt) and
628 areas of low salinity, high dissolved oxygen, and high turbidity – all indicators of glacially-
629 impacted waters. For all samples, water deeper than 10 m was less depleted in ^{18}O (average
630 $\delta^{18}\text{O}$: -1.75‰) than water above 10 m (average $\delta^{18}\text{O}$: -3.45‰). Further, surface (≥ 10 m depth)
631 samples of the “near” transect (Figure 5, top) were more depleted in ^{18}O (average $\delta^{18}\text{O}$: -4.24‰)
632 than the “distal” transect (Figure 5 bottom, average $\delta^{18}\text{O}$: -3.42‰), which in turn were more
633 depleted than surface samples collected >10 km from shore outside of the ring of moraines
634 enclosing Brae Bay (average $\delta^{18}\text{O}$: -2.18‰). These values indicate a glacial meltwater signal in
635 the marine environment which appears to be largely confined to upper 30-40 m of the water
636 column and quickly diluted within 4 km of calving front. Rising submarine discharge plumes can
637 be patchy (Andersen et al., 2010; Everett et al., 2018; Jackson et al., 2017), but using turbidity as
638 an indicator, the plume can be detected as far out as station 27, ~ 3.7 km from Sverdrup’s
639 terminus (Figure 4d). Turbidity thus corroborates the $\delta^{18}\text{O}$ picture of meltwater impacting waters
640 primarily within 4 km from the glacier front. CTD sensor measurements of dissolved oxygen
641 provide a more highly-resolved view of the potential meltwater plume and further show an
642 extended glacial influence: a “plume-like” region of elevated dissolved oxygen concentration is
643 observed within the top 20 m of the water column and extends to station 31, ~ 13 km from the
644 terminus (Figure 4c). In the “near” and “distal” transects (Figure 5c) there is evidence of a
645 subsurface plume with elevated dissolved oxygen concentrations centered at ~ 12 m depth in the
646 “near” transect, which rises (centered ~ 10 m depth) and dilutes/disperses in the “distal” transect.

647 The mapped density structure indicates that the meltwater, which enters the marine
648 environment at depth, rises to the surface within 4 km of Sverdrup’s terminus. The “plume-like”
649 feature seen in $\delta^{18}\text{O}$, salinity, dissolved oxygen, and turbidity follow the >1025 kg m^{-3} isopycnal
650 which slopes upwards from the terminus within the first 4 km of the “out” transect (Figure 4,
651 Station 22-30, white lines). Upsloping isopycnals associated with the plume along this transect
652 (i.e. those associated with densities ≤ 1026 kg m^{-3}) begin at depths ≥ 30 m depth (Figure 4); by
653 linearly extrapolating these lines of equal density back to the terminus, it appears that the plume
654 originates from depths between 30-40 m.

655 A two-component mixing model using summer marginal melt and Jones Sound deep
656 water as end-members (Sup. Table 1) was constructed to quantify the fraction of glacially-

657 derived water in marine samples and to track its extent in the near-shore environment. The model
658 uses $\delta^{18}\text{O}$ and salinity values of the most ^{18}O -depleted marginal runoff summer sample (Sup.
659 Figure 4, “MR”) and $\delta^{18}\text{O}$ and salinity values of the most ^{18}O -enriched deep marine sample (Sup.
660 Figure 4, “JS”) to calculate the fraction of glacial melt in all marine samples (Figure 6).
661 Calculations of glacial meltwater fraction are based on similar work done by Östlund and Gert
662 (1984) and Kanna et al. (2018). Surface waters (≥ 10 m) in the “near” transect have the highest
663 meltwater fractions ($\sim 12\%$ glacial melt and $\sim 88\%$ marine water on average). However, even
664 these fractions are low and the surface plume water contains significant amounts of marine water
665 even in the freshest part of the sampled plume. The meltwater fraction declines with depth,
666 where subsurface water (10-40 m below surface) averaged $\sim 6\%$ glacial melt, while deep waters
667 (>40 m below surface) contained $<5\%$ glacial melt (Figure 6). Glacial melt fraction declines with
668 distance from the glacier terminus; surface water within 4 km of shore was $\sim 12\%$ melt, while the
669 average melt fraction >4 km from shore at the surface was $\sim 7\%$. Overall the model suggests the
670 plume, as sampled, is diluted with marine water even at close proximity to the terminus; further
671 it suggests glacial melt primarily impacts near-surface waters and is diluted/dispersed efficiently
672 with distance from the terminus.

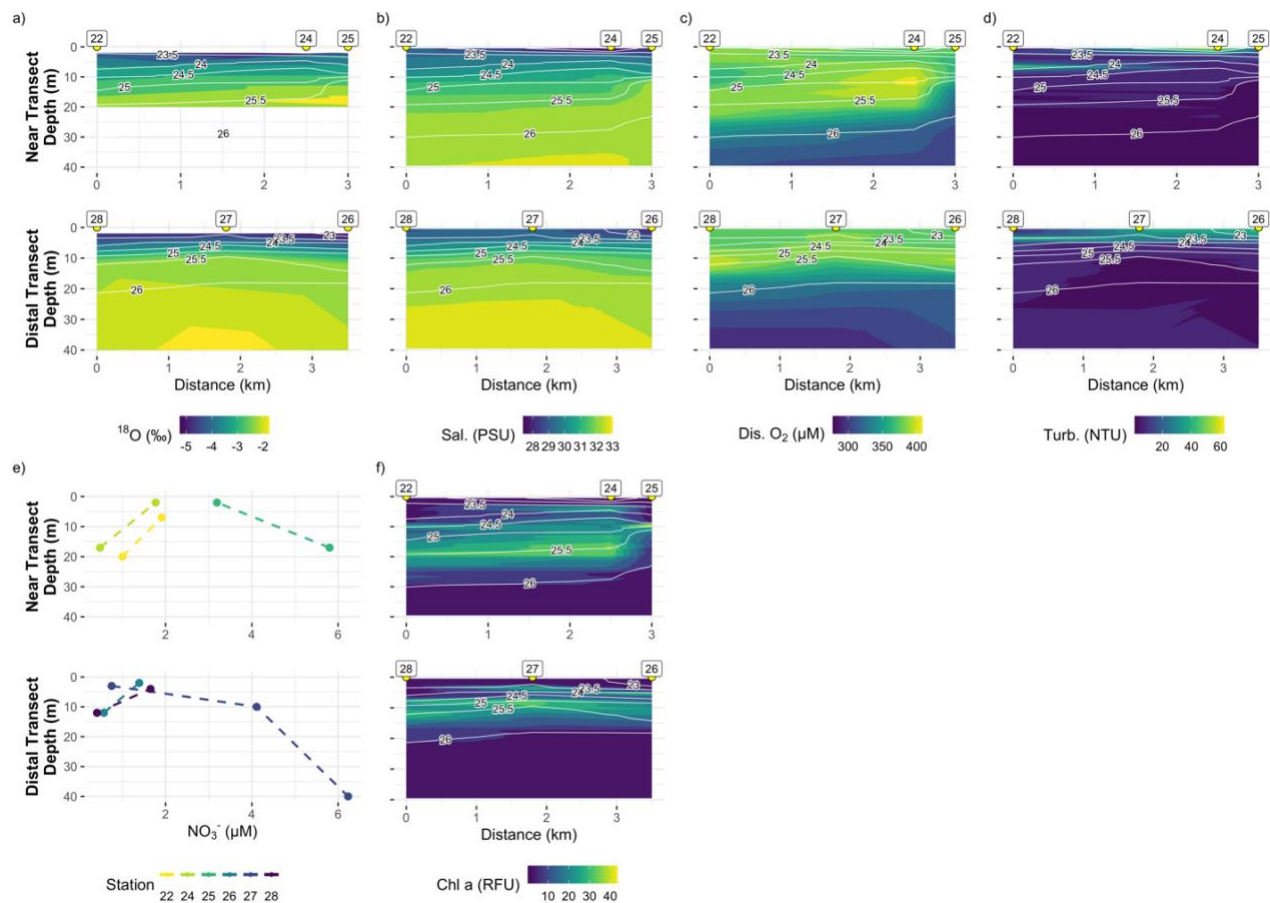


673

674 **Figure 4. Plots of (a) $\delta^{18}\text{O}$, (b) salinity, (c) dissolved oxygen concentration, (d) turbidity, (e)**
 675 **nitrate concentration, and (f) Chl *a* concentration along the “out” transect in Brae Bay.**
 676 Density anomaly (kg m^{-3}) contours are shown in white. The dotted yellow line represents
 677 euphotic depth, calculated at 0.1% of surface PAR. Only the NO_3^- concentration profile is
 678 shown, but PO_4^{3-} , and SiO_4^{4-} concentrations follow similar patterns. Station numbers are
 679 indicated at the top of the plot and distance is defined as starting at the glacier calving front.
 680 Bathymetry data (black) is from echo soundings made at each station.

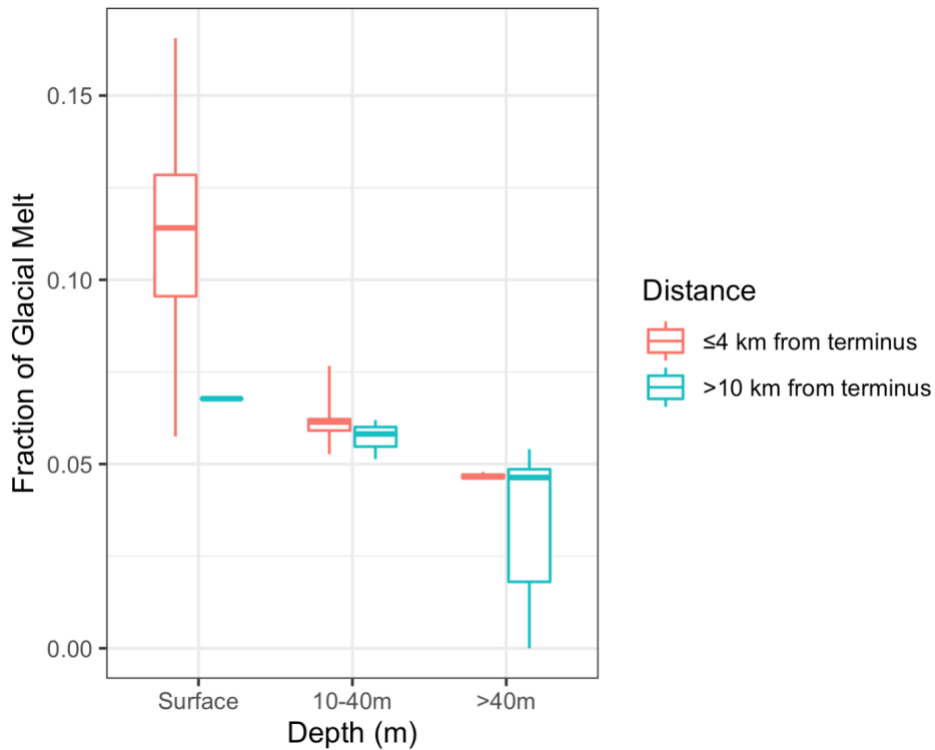
681

682



683

684 **Figure 5. Plots of (a) $\delta^{18}\text{O}$, (b) salinity, (c) dissolved oxygen concentration, (d) turbidity, (e)**
 685 **nitrate concentration, and (f) Chl *a* concentration along the “near” (top) and “distal”**
 686 **(bottom) transects in Brae Bay. Density anomaly (kg m^{-3}) contours are shown in white. Only**
 687 **the NO_3^- concentration profile is shown, but PO_4^{3-} , and SiO_4^{4-} concentrations follow similar**
 688 **patterns. Station numbers are indicated at the top of the plot and distance is defined as starting at**
 689 **the first station along the lateral transect.**



690

691 **Figure 6. Boxplot of glacial melt fractions for all samples.** The median and interquartile range
 692 for each water type are shown for marine surface water (0-10m depth), marine near-surface
 693 water (10-100m depth), and marine deep water (>100 m depth). Colors denote distance away
 694 from Sverdrup glacier’s terminal ice edge.

695

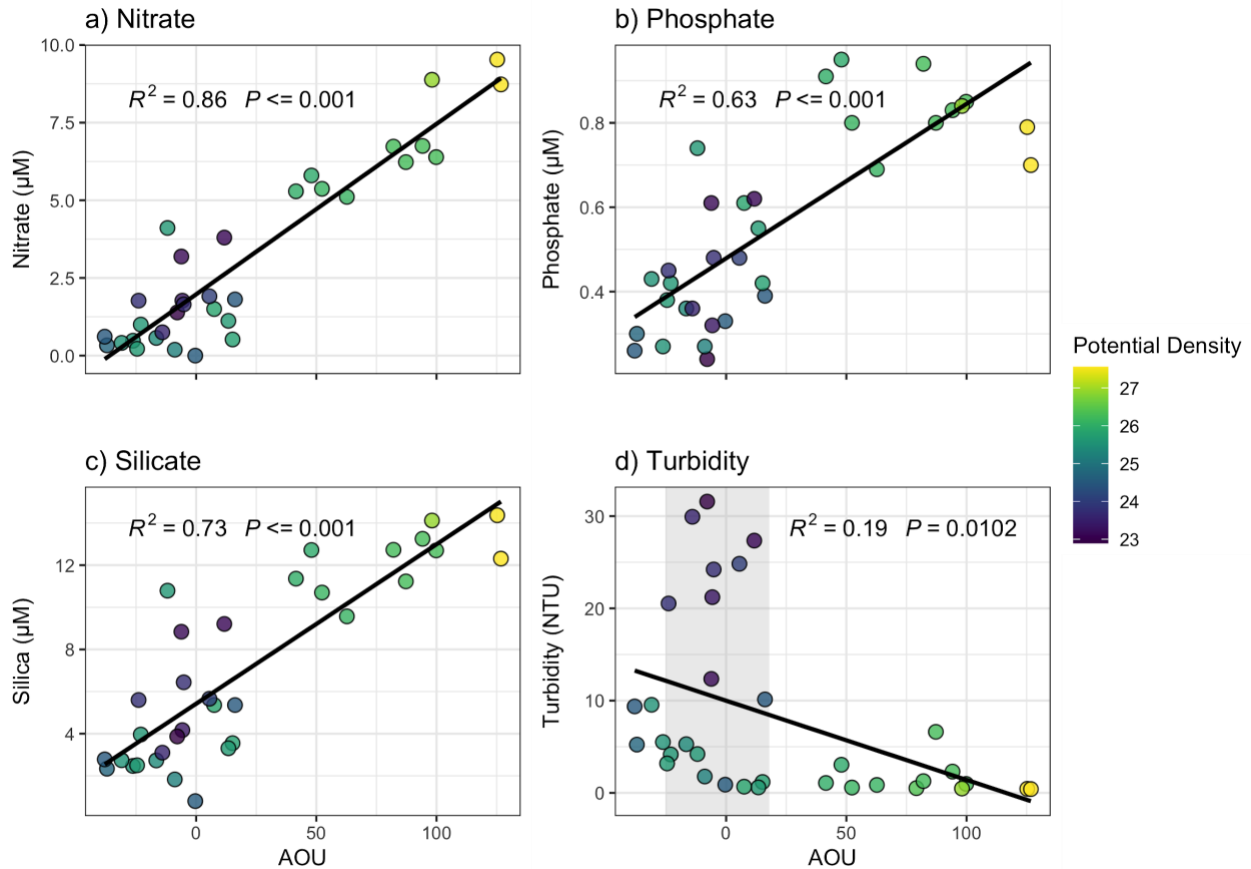
696 3.5. Meltwater impacts on the marine environment

697 Finally, the impacts of glacial input on nutrient availability, light availability, and
 698 primary production are explored via marine water column measurements. Although nutrient
 699 concentrations in glacial vs. marine samples (Table 1) show that glacial meltwater does not
 700 significantly impact near-terminus marine water nutrient concentrations, marine measurements
 701 suggest that glacial input at Sverdrup glacier does drive the delivery of marine-sourced nutrients
 702 from deeper water to the near-surface. This delivery likely occurs via entrainment in the rising
 703 meltwater plume and/or the estuarine upwelling circulation forced by the glacier’s freshwater
 704 input. The mapped density structure (Figure 4, white contours) indicates that isopycnals in the
 705 density range of 1025-1026 kg m⁻³ slope upwards towards the glacier terminus starting >26 km
 706 from the glacier. This structure provides an adiabatic pathway for marine waters at depths >60 m

707 in the open waters of Jones Sound to upwell to depths of 5-10 m in near-coastal waters in close
708 proximity to the glacier terminus. Nutrient concentrations (nitrate, phosphate, and silicate) are
709 generally lower at the surface and higher at depth (Table 1) as is typical in marine waters in the
710 late summer (Randelhoff et al., 2020). Thus, the upwelling implied by the isopycnal structure
711 likely plays a role in delivering marine waters with significant major nutrient concentrations to
712 the near-surface. Measured nutrient concentrations (Figures 4e, 5e) are consistent with this
713 scenario: nitrate concentrations are enhanced on the underside of the rising meltwater plume at
714 concentration levels consistent with those of the 1025-1026 kg m⁻³ density classes. The
715 entrainment observed at Sverdrup glacier is shallow compared to that observed at deep tidewater
716 glaciers in Greenland (Kanna et al., 2018; Meire et al., 2017) but nevertheless appears important
717 for enhancing nutrient concentrations: nutrient samples indicate that the nutricline (defined here
718 as the depth where NO₃⁻ concentrations exceed 1-μM) at all the stations within Brae Bay (≤10
719 km of the glacier terminus) occurs at or above 30 m depth. Further, average NO₃⁻ concentrations
720 in the upper 100 m of the “out” transect were higher at stations within Brae Bay (stations 22, 30,
721 27) than those farther out in Jones Sound (stations 30, 31, 32).

722 The conclusion that nutrients present in near-surface waters in close proximity to the
723 glacier terminus are marine – as opposed to glacier-sourced – is further supported by the
724 observed linear relationship between nutrient concentrations and AOU. The relationship between
725 nutrient concentrations and AOU can be used to determine if marine nutrient concentrations are
726 being impacted by direct addition of glacially-derived nutrients, as such a “disturbance” to a
727 water mass is expected to cause a departure from a linear relationship. In this system, nitrate,
728 phosphate, and silicate concentrations show linear relationships with AOU in both surface and
729 subsurface water throughout Sverdrup Bay (Figure 7a,b,c), as expected for nutrients that are deep
730 water-sourced. Expectedly, turbidity does not show this linear relationship, as turbid waters in
731 this system are glacially-sourced (Figure 7d).

732



733

734 **Figure 7. Apparent oxygen utilization (AOU) versus (a) NO_3^- , (b) PO_4^{3-} , (c) SiO_4^{4-} , and (d)**
 735 **turbidity of marine water in Sverdrup Bay.** The colour scale shows the log of depth (m). The
 736 AOU range of plume water in (d) is shown in grey.

737

738 A second important impact of glacial input on the marine environment is its impact on
 739 light availability in near-surface coastal waters in close proximity to the glacier terminus. The
 740 export of sediment-laden glacial runoff from Sverdrup Glacier into Jones Sound leads to areas of
 741 high turbidity and low light availability in the upper ~10m of the water column close (<4 km) to
 742 the freshwater outlet at the glacier terminus (Figures 4d and 5d). As a consequence, the euphotic
 743 zone (Figure 4, above the yellow dotted line) in close proximity to the terminus is influenced
 744 significantly: at station 22 (that closest to the glacier terminus) the euphotic zone depth was 9 m
 745 and it decreased to less than 5 m at stations 30 and 27 as the buoyant turbid plume rose towards
 746 the surface with distance offshore. Consistent with other indicators of the meltwater plume,
 747 which suggest that the plume is quickly diluted within 4 km of the calving front (Section 3.4),
 748 euphotic zone depths increase to over 20 m beyond a distance of ~4 km from the ice front.

749 Glacially-induced nutrient entrainment and elevated turbidity limiting light availability in
750 close proximity (within ~4km) of the terminus are likely to impact primary production in these
751 waters, although the combined net influence is not straight-forward to predict. On a large scale,
752 elevated near-surface Chl *a* concentrations were found at stations closest to the glacier front and
753 declined with depth and distance away from the glacier terminus: on average, higher Chl *a*
754 concentrations were present at all three “near” stations compared to stations on the “distal”
755 transect (Figure 6f) and Chl *a* concentrations were higher at “near” and “distal” transect stations
756 than at stations further from shore along the “out” transect (Figure 5f). On a smaller scale,
757 relationships between Chl *a* concentration, turbidity, and nutrient concentrations were variable.
758 Consistent with expectations, the least turbid and most nutrient-rich (~6 μM NO₃⁻) “near” station
759 (station 25) had the highest Chl *a* concentration (>40 RFU from CTD data). However, at many
760 stations close the glacier front (e.g. stations 22, 24, 27, and 30) the highest Chl *a* concentrations
761 (30-40 RFU from CTD data) were measured below regions of high turbidity despite the impacts
762 of the turbid plume limiting light (Figures 4d,f and 5d,f). Peaks in Chl *a* concentration at stations
763 22, 24, 26, 28 and 30 coincide with lower nutrient concentrations, while stations 25 and 27 have
764 elevated Chl *a* and nutrient concentrations (Figures 4e,f and 5e,f).

765

766 **4. Discussion**

767 **4.1. Plume dynamics in the near-shore environment**

768 At Sverdrup Glacier, a shallow, warm-based tidewater glacier in the CAA, time-lapse
769 camera imagery (Section 3.1) and *in situ* marine observations (Section 3.4) confirm the existence
770 of a freshwater plume in the near-shore marine environment tied to the glacier melt season
771 evolution. Unsurprisingly, the correlation between plume area and cumulative mass balance
772 (Sup. Figure 3) suggests that plume surface area is tied to the total volume of melt coming from
773 the glacier. It can be inferred that as the melt season progresses, a larger area of marine waters in
774 Brae Bay are impacted by glacial melt. *In situ* water samples in this study were collected when
775 the cumulative meltwater flux was near its peak (late summer), and cumulative mass balance was
776 at its most negative. It can be assumed that this sampling reflects a time of year when meltwater
777 extent in Brae Bay was likely near its maximum.

778 Results suggest that meltwater exits Sverdrup's terminus 10's of meters below the sea
779 surface. A single on-ice transect from 2009 showed the grounding line within 0.6 km of the
780 terminus to be 20 ± 10 m below the surface (Larsen, 2010). Subsequent erosion caused by
781 continued subglacial drainage likely results in the plume now exiting at even greater depth
782 (Anderson et al., 2006; Catania et al., 2018; Kessler et al., 2008). Additionally, the ice elevations
783 off the centerline are more than 10 m lower than the measured transect. These lower ice surfaces
784 are around a tunnel where subglacial melt was observed in 2019 to exit into Brae Bay (Sup.
785 Figure 1b). This depression suggests that discharge is exiting Sverdrup Glacier at a depth of >30
786 m on the eastern side of the terminus where the main plume was observed in 2019 (Figure 1c).

787 The injection of the subsurface meltwater plume has important implications for water
788 column structure in the ocean near the glacier front (Section 3.4). Near-surface (≤ 30 m depth)
789 isopycnals within 4 km of the terminus slope upwards away from the terminus, mapping the rise
790 of the buoyant plume to the surface between stations 22 (<1 km distance) and 31 (~ 13 km
791 distance). The plume's influence appears to extend down to the $1026 \text{ kg m}^{-3} \sigma_\theta$ isopycnal, and
792 extrapolation of this isopycnal's slope to the terminus indicates that the plume is originating from
793 below 40 m depth, consistent with Sverdrup's estimated grounding line depth at this point along
794 the terminus (≥ 30 m depth). This location also corresponds to the location of the main plume
795 discharge that was observed in 2019. Further offshore between 13 and 26 km from the terminus
796 (at stations 31, 32 and 33), isopycnals slope upwards towards the shore, characteristic of fjord-
797 estuarine circulation. Here, the upward-sloping isopycnals begin outside the ring of moraines that
798 hem in Brae Bay, therefore it is unlikely that this upwelling is driven directly by submarine
799 glacial discharge solely from Sverdrup Glacier. Rather, this distal upwelling could be driven by
800 variations in bathymetry (data not collected) between 4-10 km from the terminus (Timmermans
801 & Marshall, 2020) or wind-driven Ekman transport in Jones Sound (Dmitrenko et al., 2016;
802 Woodgate et al., 2005). Regardless of the forcing, this upwelling of deeper waters originating
803 from Jones Sound has important implications for nutrient transport (Section 4.5).

804

805 **4.2. Nutrient and carbon export in glacial meltwater runoff to the surface ocean**

806 It has been proposed that glacial meltwater can be a primary mechanism for the delivery
807 of macronutrients to the ocean (Hawkings et al., 2016; Hawkings et al., 2017; Tranter et al.,

2002). Our results suggest however that at Sverdrup Glacier in summer the concentrations of macronutrients in glacial meltwater runoff were not high enough to significantly augment marine concentrations. Specifically, phosphate and silicate concentrations in glacial runoff were lower than in marine water samples (Table 1). While average summer glacial and upper (>40 m depth) marine water column nitrate concentrations were not significantly different (Table 1), the volume of freshwater exported from Sverdrup Glacier over the melt season (0.34 Gt; Section 3.1) is small compared to the reservoir of receiving seawater. RACMO2.3 model results suggest that on average 5.8×10^9 L of glacial melt are delivered to the ocean each day over the 55 day summer melt season (Figure 2). Given the average nitrate concentrations in summer meltwater of $1.8 \pm 0.0 \mu\text{M}$ (Table 1), this implies an average daily nitrate delivery rate of $(1.1 \pm 0.2) \times 10^4$ mol per day. Accounting for summer plume extent, this delivery rate is estimated to impact a minimum volume of $\sim 0.01 \text{ km}^3$ of ocean water. Thus, even under the assumption of no biological uptake of nitrate, the glacial melt delivery rate is an order of magnitude too small to account for the observed 0.6-1.9 μM nitrate found in the upper 10 m of the marine water column at stations affected by the plume (Figures 4 and 5). Collectively, these results suggest that glacial melt from Sverdrup Glacier does not appreciably augment existing macronutrient concentrations in the coastal ocean distal to the ice front.

This conclusion agrees with recent studies that found direct addition via glacial meltwaters to not be a primary mechanism for delivery of macronutrients to the ocean (Cape et al., 2018; Kanna et al., 2018; Meire et al., 2017). However, debate remains, and seasonality and hydrology appear to play important roles in carbon and nutrient availability (Beaton et al., 2017; Hawkings et al., 2017; Hopwood et al., 2020). In the case of NO_3^- , a large fraction of glacially-sourced NO_3^- is derived from atmospheric deposition on the surface snowpack (Wolff, 2013), and because snow is the first to melt in summer, most of this NO_3^- is exported early in the season (Wadham et al., 2016). For example, Wadham et al. (2016) found significant concentrations of NO_3^- ($>4 \mu\text{M}$) in runoff rivers draining Leverett Glacier in samples collected before June, but by late July, NO_3^- concentrations were comparable to average concentrations observed on Sverdrup Glacier ($\sim 2 \mu\text{M}$). The low NO_3^- concentrations in the summer glacier meltwater found in this study are likely influenced by the time of sampling, i.e. at the peak of melt, when ice melt rather than snow melt dominates glacial runoff. However, should the seasonal variation of NO_3^- concentrations in meltwater from Sverdrup Glacier be of a similar magnitude to that of Leverett

839 Glacier (~2-fold difference in nutrient concentrations between early and late melt), we note that
840 seasonal variation is still insufficient for direct NO_3^- delivery rates to account for the observed
841 NO_3^- enrichment in the surface waters in Brae Bay. Further, we note that spring vs. summer
842 glacial water samples from Sverdrup Glacier do not show a large difference in NO_3^-
843 concentrations (Table 1).

844 In contrast, other studies of glaciers in Greenland have found glacial meltwater to be a
845 significant source of crustal elements, including silica (Hawkings et al., 2017; Meire et al., 2016;
846 Tranter et al., 2002) and phosphate (Hawkings et al., 2016), during peak meltwater flow. In the
847 context of these studies, our findings of low silicate and phosphate concentrations in summer
848 meltwater at Sverdrup Glacier are anomalous. The elevated concentrations of crustal elements
849 seen in the Greenland glacier studies are likely the result of bedrock geology, a prolonged melt
850 season and/or longer subglacial hydrological flow-paths, the latter two of which can result in
851 extensive water–rock interaction and enhanced physical and biologically-mediated weathering
852 (Aciego et al., 2015; Ravier & Buoncristiani, 2018). The Canadian Shield underlies both eastern
853 Devon Island and Greenland, so it is unlikely that fundamentally different bedrock geologies are
854 the cause of the variation in these macronutrient concentrations between Sverdrup Glacier and
855 the glaciers studied in Greenland. Instead, it is more likely that glacier hydrology and meltwater
856 routing played a role in generating the low meltwater nutrient concentrations observed in this
857 study (Brown, 2002). Similar to previous work (Hawkings et al., 2017; Meire et al., 2017),
858 meltwater samples here were collected in late summer, when basal hydrology is characterized by
859 fast efficient export and short rock-water interactions, limiting enrichment of crustal elements in
860 the meltwater. Phosphate and silicate concentrations in frozen spring samples were significantly
861 higher than in the summer (Table 1), and thus, these lower crustal nutrient concentrations in
862 summer melt may be evidence of low contact times. Further, on Sverdrup Glacier, most glacial
863 melt is routed marginally until just prior to the terminus. This marginal routing likely denotes
864 significantly shorter rock-water interactions with the glacier bed, explaining the lower summer
865 PO_4^{3-} , SiO_4^{4-} , and carbon concentrations observed (Bennett, 2011). Finally, Sverdrup Glacier’s
866 slow ice velocities may result in less basal erosion and a subsequent lack of crustal elements in
867 meltwater. Indeed, Milner et al. (2017) proposed that as glaciers and ice caps shrink, the quantity
868 of soluble reactive phosphorus exported in runoff decreases.

869 Similar to major nutrient concentrations, the concentration of glacial DOC was not high
870 enough for glacier meltwater inputs to significantly augment marine concentrations (Table 1).
871 However, as discussed in Section 3.3, glacier meltwater differed significantly from marine
872 waters with respect to the types of carbon present, with potentially important implications for the
873 bioavailability of DOM to support marine ecosystems. Specifically, meltwater runoff from
874 Sverdrup Glacier had a higher proportion of protein-like DOM compared to the more humic-like
875 marine DOM and based on PARAFAC and PCA analyses, protein-like DOM components (P1-
876 P3) were most associated with glacial samples. Tyrosine (P1) and tryptophan (P2) components
877 were identified by Yamashita et al. (2015) to be indicators of the bioavailability of DOM in
878 marine waters; this suggests that glacial samples from Sverdrup Glacier have a higher proportion
879 of bioavailable protein-like DOM compared to marine water samples. The P3 component is
880 related to the production of DOM via biological degradation; thus, the association between
881 spring glacial samples and P3 we find could be an indicator that protein-like DOM is a result of
882 microbially-mediated processes occurring in the basal and marginal environments (Smith et al.,
883 2018). These three protein-like components have been previously found in DOM collected from
884 Devon Island (Dubnick et al., 2017) and northern Alaska (Walker et al., 2009), as well as in
885 riverine, and to a lesser extent estuarine, waters draining the Juneau Ice Field (Fellman et al.,
886 2010b). As found in numerous other glacier studies, protein-like DOM in supraglacial and basal
887 samples (>90% protein-like) is likely the result of productive microbial communities living on
888 and under the ice that are able to generate and recycle bioavailable DOM for downstream export
889 and consumption (Bhatia et al., 2010; Hood et al., 2009; Smith et al., 2018). The elevated
890 ammonium concentrations observed here may also indicate microbial degradation of glacial
891 DOM (Kumar et al., 2016). A recent study by Dubnick et al. (2020) corroborates this, having
892 found abundant and distinct microbial communities in surface and basal ice at Sverdrup Glacier.
893 The humic-like component H1 has been found in both marine and terrestrial studies (Coble,
894 2007; De Souza Sierra et al., 1994; Stedmon et al., 2003) and has been previously observed in
895 basal ice from numerous glaciers on Devon Island (Dubnick et al., 2017). The marine humic-like
896 component H2 has also previously been found in basal ice from Devon Island (Dubnick et al.,
897 2017) and Alaska marine DOM (Walker et al., 2009). Broadly, the protein-like glacier DOM
898 found in meltwater runoff draining Sverdrup Glacier and the humic-like marine DOM found in
899 the surrounding coastal ocean is consistent with previous findings, indicating that glaciers are

900 microbially-based ecosystems capable of supplying comparatively labile DOM to downstream
901 environments (Dubnick et al., 2020; Hood et al., 2009). In the ocean, this labile DOM in glacial
902 melt can promote secondary productivity, with bacteria and microzooplankton using it as a
903 carbon source. These organisms then go on to feed higher trophic levels in the marine food web
904 (Pomeroy, 1974). Recent work in the McMurdo Dry Valleys (Antarctica) has found that
905 heterotrophic production relies on labile DOM freshly-derived from photosynthetic bacteria
906 rather than legacy organic carbon (Smith et al., 2017). While delineating the source of protein-
907 like DOM in the ocean or its relative importance to CAA heterotrophs is beyond the scope of this
908 study, if marine microbes preferentially use labile glacially-derived protein-like carbon over
909 humic-like marine carbon, as has been found in previous studies in Alaska and Colorado
910 (Arimitsu et al., 2018; Feghel et al., 2019; Fellman et al., 2015), tidewater glaciers like Sverdrup
911 Glacier, which export labile DOM to the ocean, may play an important role in stimulating local
912 secondary production in Arctic waters distal to the ice terminus during the summer months.

913

914 **4.3. Impact of the submarine discharge plume on the surface ocean**

915 While carbon and nutrient concentrations in glacial melt were not high enough to directly
916 impact the marine environment, signatures of buoyant plume rising close to the terminus (within
917 4 km) and the upwelling of deeper marine waters consistent with an estuarine-like circulation
918 farther out in Jones Sound (~13-23 km from the terminus) were both detected (Sections 3.4 and
919 3.5). In marine water unaffected by external nutrient sources, AOU will have a positive linear
920 relationship with nutrient concentration because oxygen consumption and nutrient additions have
921 a shared source: organic matter remineralization. This linear relationship is observed in Brae Bay
922 (Figure 7), further confirming that glacial melt is likely not the important source of the enriched
923 macronutrient concentrations observed in marine waters surrounding Sverdrup Glacier.

924 Previous studies of glacier-induced upwelling focus primarily on the delivery of nitrate
925 from depth, as NO_3^- is generally the limiting nutrient in the North Atlantic and Arctic oceans in
926 the summer (Randelhoff et al., 2020). Nutrient ratios in Brae Bay suggest that surface
927 phytoplankton are nitrogen limited at this time of year (Sup. Figure 5), and though upwelling at
928 Sverdrup Glacier is shallow, it occurs below the nutricline (≥ 30 m depth) and is therefore
929 sufficient to deliver waters with elevated nutrient concentrations ($\sim 5 \mu\text{M}$) to the surface. Recent

930 studies of four tidewater glaciers (Kronebreen, Kongsvegen, Conwaybreen, and Kongsbreen) in
931 Kongsfjorden (Svalbard) all with relatively shallow (≤ 70 m depth) grounding lines found similar
932 upwelled NO_3^- concentrations ($4.2 \mu\text{M}$) (Halbach et al., 2019). In comparison, deep tidewater
933 glaciers in Greenland have been shown to be capable of entraining marine water with nearly
934 double the NO_3^- concentration ($\sim 10 \mu\text{M}$) that is observed here (Kanna et al., 2018; Meire et al.,
935 2017). However, given that NO_3^- is limiting at this time of year following the spring bloom, the
936 delivery of waters with even modest concentrations of NO_3^- to the euphotic zone may promote
937 productivity. The analysis of glacial melt fraction (Section 3.4) indicated that the rising
938 meltwater plume is $\sim 13\%$ glacial melt (87% marine water), and RACMO2.3 modeling (Section
939 3.1) predicted that over the melt season Sverdrup exports a total of 0.34 Gt of meltwater to Brae
940 Bay. These estimates and measured NO_3^- concentrations thus imply that 2.0 Gt of deeper marine
941 water and $>10^{15}$ mol of NO_3^- may be delivered to surface waters during the summer – compared
942 to the <0.5 Gt of NO_3^- delivered in spring and summer glacial melt. If this delivery is typical of
943 the over 300 tidewater glaciers in the CAA, this implies that tidewater glaciers in this region may
944 be responsible for delivering >3 Gt of NO_3^- to the surface ocean annually. It should be noted that
945 the differences in underlying geology of CAA glaciers likely makes this estimation highly
946 uncertain. Further, while most tidewater glaciers in the CAA have shallow discharge plumes
947 relative to glaciers in Greenland, Sverdrup Glacier is an example of a very shallow tidewater
948 glacier, even for the CAA (Cook et al., 2019), and thus, this estimate may be an underestimation.
949 Regardless, this value represents nearly 2x more nitrate than is exported by the Mackenzie River
950 in a year (Holmes et al., 2011). Note, however, that riverine input represents a source of ‘new’
951 nitrogen to the marine environment while glacially-derived upwelling redistributes marine
952 nitrogen. Both are important for supporting productivity, but only ‘new’ nitrogen can alter the
953 total marine nitrogen budget.

954

955 **4.4. Glacier effects on primary productivity in front of a shallow tidewater glacier**

956 Past studies of glaciers in Greenland and Svalbard have observed elevated surface
957 concentrations of Chl *a* associated with regions of glacially-driven upwelling of nutrient-rich
958 marine waters (Halbach et al., 2019; Kanna et al., 2018; Meire et al., 2017). Here, peaks in Chl *a*
959 concentrations are primarily found within (stations 22, 30) or at the edges (station 24 and 25) of

960 the turbid meltwater plume in Brae Bay (Figures 4 and 5). The presence of high Chl *a*
961 concentrations in areas of low nutrient concentrations suggests the biological uptake of
962 macronutrients. Higher Chl *a* concentrations at all three “near” stations compared to the stations
963 on the “distal” and “out” transects suggest that the strongest biological response to the buoyant
964 meltwater plume upwelling occurs within 1 km of the terminus, where entrained nutrient-rich
965 marine water is delivered to the surface. We also observe elevated Chl *a* concentrations ~13 km
966 from the terminus (station 31) in an area of upwelling of deeper marine waters outside of the
967 moraines hemming Brae Bay. It is unlikely that this estuarine-like upwelling >10 km from
968 Sverdrup’s terminus is wholly dependent on subglacial discharge exiting at ≥ 30 m depth from
969 the terminus of Sverdrup Glacier, but freshwater delivery along the coast may play an important
970 role in driving estuarine-like circulation. Regardless, the distal upwelling does appear to
971 promote the delivery of nutrient-rich water to the surface farther out in Jones Sound, sustaining
972 elevated Chl *a* concentrations compared to surface waters >20 km from Sverdrup.

973 The Chl *a* responses seen in the Sverdrup Glacier system differ from those reported in
974 studies on larger Greenland glaciers in important respects; specifically, the response is less
975 extreme and spatial extent more limited at Sverdrup Glacier. Maximum Chl *a* concentration at
976 Sverdrup was ~7.5 $\mu\text{g/L}$ (extracted concentration), while concentrations in previous studies in
977 Greenland can exceed 20 $\mu\text{g/L}$ (Meire et al., 2017). These relatively small Chl *a* enhancements
978 appear consistent with shallower tidewater glacier systems. Recent work at shallow tidewater
979 glaciers in Svalbard report maximum Chl *a* concentrations of ~2.8 $\mu\text{g/L}$ (Halbach et al., 2019)
980 during late July and early August. The different Chl *a* concentrations observed between these
981 studies does not directly follow differences in glacier grounding line and submarine discharge
982 depths, as current models would predict (Hopwood et al., 2018; Oliver et al., 2020). That being
983 said, model values are not directly comparable to single point in time Chl *a* measurements, so
984 more work and samples are necessary to fully evaluate how measured Chl *a* compare to modeled
985 productivity estimates. Meire et al. (2017), observed high (~20 $\mu\text{g/L}$) Chl *a* concentrations at
986 glaciers with deeper grounding lines (≥ 140 m depth) than Sverdrup, lower turbidities (<15
987 NTU), and a deeper euphotic zone than Sverdrup Glacier. However, the proximity of the closest
988 Chl *a* measurement in that study was almost 10 km away from the glacier terminus, making
989 direct comparisons to this work difficult. At Bowdoin glacier (in Greenland), however, Kanna et
990 al., (2018) collected samples within 1 km of the terminus, finding similar proportions of glacial

991 melt in the plume water at that site (14%) as found here (13%). There, the highest observed Chl *a*
992 (~6.5 µg/L) are similar to the maximum concentrations observed in this study (~7.5 µg/L). This
993 is surprising, considering that Sverdrup has an estimated grounding line of >30 m depth
994 compared to >200 m depth at Bowdoin Glacier. However, Kanna et al. (2018) did find elevated
995 Chl *a* concentrations nearly 20 km into Bowdoin Fiord, while we see an elevated Chl *a* response
996 extending a maximum of ~13.3 km from Sverdrup's terminus. The confined walls of Bowdoin
997 fjord, different meltwater fluxes, and deeper grounding line may induce a larger degree of
998 circulation, promoting similar levels of productivity farther away from the glacier terminus in the
999 case of Bowdoin Glacier relative to Sverdrup Glacier. In Kongsfjorden (Svalbard), at both
1000 Kronebreen and Kongsvegen glaciers (discharge ~70 m depth) and Conwaybreen and
1001 Kongsbreen glaciers (discharge <10 m depth), Chl *a* concentrations were universally low
1002 (Halbach et al., 2019). In these cases, the marine waters around the deeper (~70 m depth)
1003 glaciers had lower Chl *a* concentrations (0.2–1.9 µg/L) likely due to higher turbidity, with
1004 differences in particle size and type (carbonate vs. silicates) between the sites playing an
1005 important role in light limitation. Thus, the “productivity continuum” between land terminating
1006 and tidewater glaciers, as defined by grounding line depth, does not appear to entirely hold for
1007 shallow tidewater glacier systems. Indeed, productivity at Sverdrup Glacier may be similar to or
1008 higher than productivity at other glaciers with deeper grounding lines (Halbach et al., 2019;
1009 Kanna et al., 2018). However, more study is clearly necessary to understand the full range of
1010 controls on entrainment, upwelling, nutrient delivery, and productivity at shallow tidewater
1011 glaciers.

1012

1013 **5. Conclusion**

1014 Historically, tidewater glaciers have been identified as areas of heightened productivity
1015 (Lydersen et al., 2014; Vibe, 1939). Recently, glacially-induced upwelling of nutrient-rich deep
1016 water has been proposed as a mechanism that can support primary productivity at the termini of
1017 tidewater glaciers in Alaska, Greenland, Svalbard, and Antarctica (Arimitsu et al., 2016;
1018 Lydersen et al., 2014; Meire et al., 2017). No study has been conducted on this topic in the CAA
1019 in almost 50 years (Apollonio, 1973). Here we find that carbon and nutrient concentrations in
1020 glacial melt are too low to enrich surface marine concentrations in the coastal ocean. However,

1021 similar to other studies, glacially-derived organic carbon exported within submarine discharge
1022 appears to be more bioavailable than marine carbon in the receiving seawater. We also observe
1023 that as the submarine discharge plume rises at the terminal ice cliff, it impacts the hydrography
1024 of the surrounding water column, inducing upwelling of intermediate (>30 m depth) marine
1025 water with elevated nutrient concentrations. The heightened Chl *a* concentrations observed at the
1026 interface between turbid freshened water and upwelled marine water close to the glacier terminus
1027 suggests that tidewater glaciers with shallow submarine outlets can promote primary productivity
1028 during nutrient-limited times of year.

1029 Based on nutrient concentrations and Chl *a* response, Sverdrup Glacier falls between
1030 deep tidewater and land terminating glaciers, while it lies near the shallow end of the spectrum of
1031 grounding line depths (Hopwood et al., 2018). Compared to many glaciers examined in previous
1032 studies, Sverdrup Glacier is less dynamic, with a smaller meltwater flux and a shallower depth of
1033 submarine discharge. However, within 4 km of its terminus, the marine waters distal to Sverdrup
1034 Glacier may be as productive as tidewater glaciers in Svalbard and Greenland with deeper
1035 grounding lines (Halbach et al., 2019; Kanna et al., 2018). The differences between deep and
1036 shallow tidewater glaciers in the magnitude and variability of observed nutrient and Chl *a*
1037 concentrations speak to the importance of determining the impacts of runoff on a variety of
1038 proglacial aquatic environments. Further, simultaneous measurements of carbon and
1039 macronutrients in both on-ice and marine environments allowed us to detect glacially-induced
1040 entrainment of deep water and estuarine upwelling in Brae Bay, while confirming that glacial
1041 concentrations were too low to augment downstream nutrient and carbon pools. With continued
1042 retreat of large tidewater glaciers in Arctic seas, future work on how shallow tidewater glaciers
1043 affect downstream marine ecosystems will only become more relevant to the region as a whole.

1044

1045 **Acknowledgments, Samples, and Data**

1046 We thank Ashley Dubnick, Brad Danielson, and Clare Bernard-Grand'Maison for assistance in
1047 the field on Devon Island. A special thanks to the Brossier family, Maria Cavaco for assistance
1048 with field preparation, Brad Danielson for assistance with the time-lapse camera imagery
1049 processing, Martin Sharp, Paul Myers, and Vince St. Louis for useful discussions and edits, and
1050 Jimmy Qaapik and the Hamlet of Grise Fiord for assistance in the field and invaluable feedback

1051 and advice. This research was funded by NFRF Explorations Fund Grant NFRFE-2018-01427 to
1052 E. Bertrand, M. Bhatia, S. Waterman, and J. Qaapik. NSERC Shiptime (RGPST-544982-2020)
1053 to J. Halfar and P. Myers, Polar Continental Shelf Project (PCSP) grant 68719 to M. Bhatia,
1054 Canada Research Chairs to E. Bertrand and S. Waterman, and a Campus Alberta Innovation
1055 Program Chair to M. Bhatia. Support to D. Burgess provided through the Climate Change
1056 Geoscience Program, Lands and Minerals Sector, Natural Resources Canada. Data is available
1057 via the Polar Data Catalogue (<https://www.polardata.ca>) CCID: 13211.

1058

1059 **References**

1060

- 1061 Aciego, S. M., Stevenson, E. I., & Arendt, C. A. (2015). Climate versus geological controls on glacial meltwater
 1062 micronutrient production in southern Greenland. *Earth and Planetary Science Letters*, 424, 51-58.
 1063 doi:10.1016/j.epsl.2015.05.017
- 1064 Andersen, M. L., Larsen, T. B., Nettles, M., Eløsegui, P., van As, D., Hamilton, G. S., . . . Dahl-Jensen, D. (2010).
 1065 Spatial and temporal melt variability at Helheim Glacier, East Greenland, and its effect on ice dynamics.
 1066 *Journal of Geophysical Research*, 115(F4), 6886-6894. doi:10.1029/2010jf001760
- 1067 Anderson, R. S., Molnar, P., & Kessler, M. A. (2006). Features of glacial valley profiles simply explained. *Journal*
 1068 *of Geophysical Research*, 111(F1). doi:<https://doi.org/10.1029/2005JF000344>
- 1069 Apollonio, S. (1973). Glaciers and nutrients in arctic seas. *Science*, 180(4085), 491-493.
 1070 doi:10.1126/science.180.4085.491
- 1071 Arar, E. J., & Collins, G. B. (1997). *Method 445.0 In Vitro Determination of Chlorophyll a and Pheophytin in*
 1072 *Marine and Freshwater Algae by Fluorescence*. Retrieved from Washington, DC:
- 1073 Arimitsu, M. L., Hobson, K. A., Webber, D. N., Piatt, J. F., Hood, E. W., & Fellman, J. B. (2018). Tracing
 1074 biogeochemical subsidies from glacier runoff into Alaska's coastal marine food webs. *Glob Chang Biol*,
 1075 24(1), 387-398. doi:10.1111/gcb.13875
- 1076 Arimitsu, M. L., Piatt, J. F., & Mueter, F. (2016). Influence of glacier runoff on ecosystem structure in Gulf of
 1077 Alaska fjords. *Marine Ecology Progress Series*, 560, 19-40. doi:10.3354/meps11888
- 1078 Azam, F., & Malfatti, F. (2007). Microbial structuring of marine ecosystems. *Nat Rev Microbiol*, 5(10), 782-791.
 1079 doi:10.1038/nrmicro1747
- 1080 Barber, F. G., & Huyer, A. (1977). *On the oceanography of Jones Sound, NWT*. Retrieved from Ottawa, Ontario,
 1081 Canada:
- 1082 Beaton, A. D., Wadham, J. L., Hawkings, J., Bagshaw, E. A., Lamarche-Gagnon, G., Mowlem, M. C., & Tranter,
 1083 M. (2017). High-Resolution in Situ Measurement of Nitrate in Runoff from the Greenland Ice Sheet.
 1084 *Environ Sci Technol*, 51(21), 12518-12527. doi:10.1021/acs.est.7b03121
- 1085 Bennett, M. R. (2011). Ice-Marginal Processes. In S. V.P., S. P., & H. U.K. (Eds.), *Encyclopedia of Snow, Ice and*
 1086 *Glaciers* (Vol. Encyclopedia of Earth Sciences Series). Dordrecht: Springer.
- 1087 Benson, B. B., & Krause, D. (1984). The concentration and isotopic fractionation of oxygen dissolved in freshwater
 1088 and seawater in equilibrium with the atmosphere I. *Limnology and Oceanography*, 29(3), 620-632.
 1089 doi:10.4319/lo.1984.29.3.0620
- 1090 Bhatia, M. P., Das, S. B., Longnecker, K., Charette, M. A., & Kujawinski, E. B. (2010). Molecular characterization
 1091 of dissolved organic matter associated with the Greenland ice sheet. *Geochimica et Cosmochimica Acta*,
 1092 74, 3768-3784. doi:10.1016/j.gca.2010.03.035
- 1093 Bhatia, M. P., Das, S. B., Xu, L., Charette, M. A., Wadham, J. L., & Kujawinski, E. B. (2013a). Organic carbon
 1094 export from the Greenland ice sheet. *Geochimica et Cosmochimica Acta*, 109, 329-344.
 1095 doi:10.1016/j.gca.2013.02.006
- 1096 Bhatia, M. P., Kujawinski, E. B., Das, S. B., Breier, C. F., Henderson, P. B., & Charette, M. A. (2013b). Greenland
 1097 meltwater as a significant and potentially bioavailable source of iron to the ocean. *Nature Geoscience*, 6,
 1098 274-278. doi:10.1038/ngeo1746
- 1099 Błaszczyk, M., Jania, J. A., & Hagen, J. O. (2009). Tidewater glaciers of Svalbard: Recent changes and estimates of
 1100 calving fluxes. *Polish Polar Research*, 30(2), 85-102.
- 1101 Boon, S., & Sharp, M. (2003). The role of hydrologically-driven ice fracture in drainage system evolution on an
 1102 Arctic glacier. *Geophysical Research Letters*, 30(18), 1916-1919. doi:10.1029/2003gl018034
- 1103 Box, J. E., Colgan, W. T., Wouters, B., Burgess, D. O., O'Neel, S., Thomson, L. I., & Mernild, S. H. (2018). Global
 1104 sea-level contribution from Arctic land ice: 1971–2017. *Environmental Research Letters*, 13(12), 125012.
 1105 doi:10.1088/1748-9326/aaf2ed
- 1106 Boyd, E. S., Lange, R. K., Mitchell, A. C., Havig, J. R., Hamilton, T. L., Lafreniere, M. J., . . . Skidmore, M. (2011).
 1107 Diversity, abundance, and potential activity of nitrifying and nitrate-reducing microbial assemblages in a
 1108 subglacial ecosystem. *Appl Environ Microbiol*, 77(14), 4778-4787. doi:10.1128/AEM.00376-11
- 1109 Bro, R. (1997). PARAFAC. Tutorial and applications. *Chemometrics and Intelligent Laboratory Systems*, 38(2),
 1110 149-171. doi:10.1016/s0169-7439(97)00032-4
- 1111 Brown, G. H. (2002). Glacier meltwater hydrochemistry. *Applied Geochemistry*, 17(7), 855-883. doi:10.1016/s0883-
 1112 2927(01)00123-8

1113 Burgess, D. O. (2018). Validation of the RACMO2.3 surface mass-balance model over northwest Devon Ice Cap,
1114 Nunavut. *Geological Survey of Canada, Open File 8382*, 1-19. doi:10.4095/308355

1115 Cape, M. R., Straneo, F., Beird, N., Bundy, R. M., & Charette, M. A. (2018). Nutrient release to oceans from
1116 buoyancy-driven upwelling at Greenland tidewater glaciers. *Nature Geoscience*, *12*(1), 34-39.
1117 doi:10.1038/s41561-018-0268-4

1118 Catania, G. A., Stearns, L. A., Sutherland, D. A., Fried, M. J., Bartholomaus, T. C., Morlighem, M., . . . Nash, J.
1119 (2018). Geometric Controls on Tidewater Glacier Retreat in Central Western Greenland. *Journal of*
1120 *Geophysical Research: Earth Surface*, *123*(8), 2024-2038. doi:10.1029/2017jf004499

1121 CHS Nautical Chart 7310, S. (Cartographer). (2011). Jones Sound Nautical Chart 7310

1122 Coble, P. G. (1996). Characterization of marine and terrestrial DOM in seawater using excitation-emission matrix
1123 spectroscopy. *Marine Chemistry*, *51*(4), 325-346. doi:10.1016/0304-4203(95)00062-3

1124 Coble, P. G. (2007). Marine optical biogeochemistry: the chemistry of ocean color. *Chem Rev*, *107*(2), 402-418.
1125 doi:10.1021/cr050350+

1126 Cook, A. J., Copland, L., Noel, B. P. Y., Stokes, C. R., Bentley, M. J., Sharp, M. J., . . . van den Broeke, M. R.
1127 (2019). Atmospheric forcing of rapid marine-terminating glacier retreat in the Canadian Arctic
1128 Archipelago. *Sci Adv*, *5*(3), eaau8507. doi:10.1126/sciadv.aau8507

1129 Cress, P., & Wyness, R. (1961). The Devon Island Expedition: Observations of glacial movements. *ARCTIC*, *14*,
1130 257-259.

1131 Cutter, G. A., & Bruland, K. W. (2012). Rapid and noncontaminating sampling system for trace elements in global
1132 ocean surveys. *Limnology and Oceanography: Methods*, *10*(6), 425-436. doi:10.4319/lom.2012.10.425

1133 Das, S. B., Joughin, I., Behn, M. D., Howat, I. M., King, M. A., Lizarralde, D., & Bhatia, M. P. (2008). Fracture
1134 propagation to the base of the Greenland Ice Sheet during supraglacial lake drainage. *Science*, *320*(5877),
1135 778-781. doi:10.1126/science.1153360

1136 De Souza Sierra, M. M., Donard, O. F. X., Lamotte, M., Belin, C., & Ewald, M. (1994). Fluorescence spectroscopy
1137 of coastal and marine waters. *Marine Chemistry*, *47*(2), 127-144. doi:10.1016/0304-4203(94)90104-x

1138 Dmitrenko, I., Kirillov, S., Tremblay, B., Gratton, Y., Barber, D., & Rysgaard, S. (2016). Upwelling of Atlantic
1139 Water along the Canadian Beaufort Sea Continental Slope: Favorable Atmospheric Conditions and
1140 Seasonal and Interannual Variations. *Journal of Climate*, *29*(12), 4509-4523. doi:10.1175/jcli-d-15-0804.1

1141 Dowdeswell, J. A., Benham, T. J., Gorman, M. R., Burgess, D., & Sharp, M. J. (2004). Form and flow of the Devon
1142 Island Ice Cap, Canadian Arctic. *Journal of Geophysical Research: Earth Surface*, *109*, F02002.
1143 doi:10.1029/2003JF000095

1144 Dubnick, A., Barker, J., Sharp, M., Wadham, J., Lis, G., Telling, J., . . . Jackson, M. (2017). Characterization of
1145 dissolved organic matter (DOM) from glacial environments using total fluorescence spectroscopy and
1146 parallel factor analysis. *Annals of Glaciology*, *51*(56), 111-122. doi:10.3189/172756411795931912

1147 Dubnick, A., Sharp, M., Danielson, B., Saidi-Mehrabad, A., & Barker, J. (2020). Basal thermal regime affects the
1148 biogeochemistry of subglacial systems. *Biogeosciences*, *17*(4), 963-977. doi:10.5194/bg-17-963-2020

1149 Etherington, L. L., Hooge, P. N., Hooge, E. R., & Hill, D. F. (2007). Oceanography of Glacier Bay, Alaska:
1150 Implications for biological patterns in a glacial fjord estuary. *Estuaries and Coasts*, *30*(6), 927-944.
1151 doi:10.1007/bf02841386

1152 Everett, A., Kohler, J., Sundfjord, A., Kovacs, K. M., Torsvik, T., Pramanik, A., . . . Lydersen, C. (2018). Subglacial
1153 discharge plume behaviour revealed by CTD-instrumented ringed seals. *Sci Rep*, *8*(1), 13467.
1154 doi:10.1038/s41598-018-31875-8

1155 Fegel, T., Boot, C. M., Broeckling, C. D., Baron, J. S., & Hall, E. K. (2019). Assessing the Chemistry and
1156 Bioavailability of Dissolved Organic Matter From Glaciers and Rock Glaciers. *Journal of Geophysical*
1157 *Research: Biogeosciences*, *124*(7), 1988-2004. doi:10.1029/2018jg004874

1158 Fellman, J. B., Hood, E., Raymond, P. A., Hudson, J., Bozeman, M., & Arimitsu, M. (2015). Evidence for the
1159 assimilation of ancient glacier organic carbon in a proglacial stream food web. *Limnology and*
1160 *Oceanography*, *60*(4), 1118-1128. doi:10.1002/lno.10088

1161 Fellman, J. B., Hood, E., & Spencer, R. G. M. (2010a). Fluorescence spectroscopy opens new windows into
1162 dissolved organic matter dynamics in freshwater ecosystems: A review. *Limnology and Oceanography*,
1163 *55*(6), 2452-2462. doi:10.4319/lo.2010.55.6.2452

1164 Fellman, J. B., Spencer, R. G. M., Hernes, P. J., Edwards, R. T., D'Amore, D. V., & Hood, E. (2010b). The impact
1165 of glacier runoff on the biodegradability and biochemical composition of terrigenous dissolved organic
1166 matter in near-shore marine ecosystems. *Marine Chemistry*, *121*(1-4), 112-122.
1167 doi:10.1016/j.marchem.2010.03.009

1168 Flowers, G. E. (2015). Modelling water flow under glaciers and ice sheets. *Proceedings of the Royal Society A: Mathematical, Physical and Engineering Sciences*, 471, 20140907. doi:10.1098/rspa.2014.0907

1169

1170 Garcia, H. E., Locarnini, R. A., Boyer, T. P., Antonov, J. I., Mishonov, A. V., Baranova, O. K., . . . Johnson, D. R.

1171 (2013). *World Ocean Atlas 2013. Vol. 3: Dissolved Oxygen, Apparent Oxygen Utilization, and Oxygen*

1172 *Saturation* (A. Mishonov Ed. Vol. NOAA Atlas NESDIS).

1173 Gray, L. (2005). Evidence for subglacial water transport in the West Antarctic Ice Sheet through three-dimensional

1174 satellite radar interferometry. *Geophysical Research Letters*, 32, L03501. doi:10.1029/2004gl021387

1175 Halbach, L., Vihtakari, M., Duarte, P., Everett, A., Granskog, M. A., Hop, H., . . . Assmy, P. (2019). Tidewater

1176 Glaciers and Bedrock Characteristics Control the Phytoplankton Growth Environment in a Fjord in the

1177 Arctic. *Frontiers in Marine Science*, 6, 254. doi:10.3389/fmars.2019.00254

1178 Hartley, C. H., & Dunbar, M. J. (1938). On the hydrographic mechanism of the so-called brown zones associated

1179 with tidal glaciers. *Journal of Marine Research*, 1, 305.

1180 Hawkings, J., Wadham, J., Tranter, M., Telling, J., Bagshaw, E., Beaton, A., . . . Nienow, P. (2016). The Greenland

1181 Ice Sheet as a hot spot of phosphorus weathering and export in the Arctic. *Global Biogeochemical Cycles*,

1182 30, 191-210. doi:10.1002/2015GB005237

1183 Hawkings, J. R., Wadham, J. L., Benning, L. G., Hendry, K. R., Tranter, M., Tedstone, A., . . . Raiswell, R. (2017).

1184 Ice sheets as a missing source of silica to the polar oceans. *Nature Communications*, 8, 14198.

1185 doi:10.1038/ncomms14198

1186 Hawkings, J. R., Wadham, J. L., Tranter, M., Lawson, E., Sole, A., Cowton, T., . . . Telling, J. (2015). The effect of

1187 warming climate on nutrient and solute export from the Greenland Ice Sheet. *Geochemical Perspectives*

1188 *Letters*, 94-104. doi:10.7185/geochemlet.1510

1189 Holmes, R. M., McClelland, J. W., Peterson, B. J., Tank, S. E., Bulygina, E., Eglinton, T. I., . . . Zimov, S. A.

1190 (2011). Seasonal and Annual Fluxes of Nutrients and Organic Matter from Large Rivers to the Arctic

1191 Ocean and Surrounding Seas. *Estuaries and Coasts*, 35(2), 369-382. doi:10.1007/s12237-011-9386-6

1192 Hood, E., Fellman, J., Spencer, R. G. M., Hernes, P. J., Edwards, R., D'Amore, D., & Scott, D. (2009). Glaciers as a

1193 source of ancient and labile organic matter to the marine environment. *Nature*, 462, 1044-1047.

1194 doi:10.1038/nature08580

1195 Hopwood, M. J., Carroll, D., Browning, T. J., Meire, L., Mortensen, J., Krisch, S., & Achterberg, E. P. (2018). Non-

1196 linear response of summertime marine productivity to increased meltwater discharge around Greenland.

1197 *Nature Communications*, 9, 3256. doi:10.1038/s41467-018-05488-8

1198 Hopwood, M. J., Carroll, D., Dunse, T., Hodson, A., Holding, J. M., Iriarte, J. L., . . . Meire, L. (2020). Review

1199 Article: How does glacier discharge affect marine biogeochemistry and primary production in the Arctic?

1200 *The Cryosphere Discussions*. doi:10.5194/tc-2019-136

1201 Hubbard, B. P., Sharp, M. J., Willis, I. C., Nielsen, M. K., & Smart, C. C. (1995). Borehole water-level variations

1202 and the structure of the subglacial hydrological system of Haut Glacier d'Arolla, Valais, Switzerland.

1203 *Journal of Glaciology*, 41(139), 572-583. doi:10.3189/s0022143000034894

1204 Jackson, R. H., Shroyer, E. L., Nash, J. D., Sutherland, D. A., Carroll, D., Fried, M. J., . . . Stearns, L. A. (2017).

1205 Near-glacier surveying of a subglacial discharge plume: Implications for plume parameterizations.

1206 *Geophysical Research Letters*, 44(13), 6886-6894. doi:10.1002/2017gl073602

1207 Juul-Pedersen, T., Arendt, K. E., Mortensen, J., Blicher, M. E., Søgaard, D. H., & Rysgaard, S. (2015). Seasonal and

1208 interannual phytoplankton production in a sub-Arctic tidewater outlet glacier fjord, SW Greenland. *Marine*

1209 *Ecology Progress Series*, 524, 27-38. doi:10.3354/meps11174

1210 Kanna, N., Sugiyama, S., Ohashi, Y., Sakakibara, D., Fukamachi, Y., & Nomura, D. (2018). Upwelling of

1211 Macronutrients and Dissolved Inorganic Carbon by a Subglacial Freshwater Driven Plume in Bowdoin

1212 Fjord, Northwestern Greenland. *Journal of Geophysical Research: Biogeosciences*, 123, 1666-1682.

1213 doi:10.1029/2017JG004248

1214 Keeler, C. M. (1964). Relationship between climate, ablation, and runoff on the Sverdrup Glacier 1963, Devon

1215 Island, NWT. *Montreal: Arctic Institute of North America, Research Paper 27*, 125.

1216 Kessler, M. A., Anderson, R. S., & Briner, J. P. (2008). Fjord insertion into continental margins driven by

1217 topographic steering of ice. *Nature Geoscience*, 1(6), 365-369. doi:10.1038/ngeo201

1218 Koerner, R. M. (1970). The Mass Balance of the Devon Island Ice Cap, Northwest Territories, Canada, 1961-66.

1219 *Journal of Glaciology*, 9(57), 325-336. doi:10.3189/s0022143000022863

1220 Koerner, R. M., Apollonio, S., Cowie, J. W., Voegtli, K., Cress, P., Wyness, R., & Greenhouse, J. P. (1961). The

1221 Devon Island Expedition. *ARCTIC*, 14(4). doi:10.14430/arctic3683

1222 Kumar, V., Tiwari, M., Nagoji, S., & Tripathi, S. (2016). Evidence of Anomalously Low delta(13)C of Marine

1223 Organic Matter in an Arctic Fjord. *Sci Rep*, 6, 36192. doi:10.1038/srep36192

1224 Larsen, C. (2010). *IceBridge UAF Lidar Profiler LIB Geolocated Surface Elevation Triplets, Version 1*.

1225 Lydersen, C., Assmy, P., Falk-Petersen, S., Kohler, J., Kovacs, K. M., Reigstad, M., . . . Zajaczkowski, M. (2014).

1226 The importance of tidewater glaciers for marine mammals and seabirds in Svalbard, Norway. *Journal of*

1227 *Marine Systems*, 129, 452-471. doi:10.1016/j.jmarsys.2013.09.006

1228 McDougal, T. J., & Barker, P. M. (2011). *Getting started with TEOS-10 and the Gibbs Seawater (GSW)*

1229 *Oceanographic Toolbox: SCOR/IAPSO WG127*.

1230 Meire, L., Mortensen, J., Meire, P., Juul-Pedersen, T., Sejr, M. K., Rysgaard, S., . . . Meysman, F. J. R. (2017).

1231 Marine-terminating glaciers sustain high productivity in Greenland fjords. *Global Change Biology*, 23,

1232 5344-5357. doi:10.1111/gcb.13801

1233 Meire, L., Mortensen, J., Rysgaard, S., Bendtsen, J., Boone, W., Meire, P., & Meysman, F. J. R. (2016). Spring

1234 bloom dynamics in a subarctic fjord influenced by tidewater outlet glaciers (Godthåbsfjord, SW

1235 Greenland). *Journal of Geophysical Research: Biogeosciences*, 121(6), 1581-1592.

1236 doi:10.1002/2015jg003240

1237 Meire, L., Søgaard, D. H., Mortensen, J., Meysman, F. J. R., Soetaert, K., Arendt, K. E., . . . Rysgaard, S. (2015).

1238 Glacial meltwater and primary production are drivers of strong CO₂ uptake in

1239 fjord and coastal waters adjacent to the Greenland Ice Sheet. *Biogeosciences*, 12(8), 2347-2363.

1240 doi:10.5194/bg-12-2347-2015

1241 Melling, H., Agnew, T. A., Falkner, K. K., Greenberg, D. A., Lee, C. M., Münchow, A., . . . Woodgate, R. A.

1242 (2008). Fresh-Water Fluxes via Pacific and Arctic Outflows Across the Canadian Polar Shelf. In R. R.

1243 Dickson, J. Meincke, & P. Rhines (Eds.), *Arctic-Subarctic Ocean Fluxes: Defining the Role of the*

1244 *Northern Seas in Climate* (pp. 193-247). Dordrecht: Springer Netherlands.

1245 Milner, A. M., Khamis, K., Battin, T. J., Brittain, J. E., Barrand, N. E., Fureder, L., . . . Brown, L. E. (2017). Glacier

1246 shrinkage driving global changes in downstream systems. *Proc Natl Acad Sci U S A*, 114(37), 9770-9778.

1247 doi:10.1073/pnas.1619807114

1248 Morlighem, M., Williams, C. N., Rignot, E., An, L., Arndt, J. E., Bamber, J. L., . . . Zinglensen, K. B. (2017).

1249 BedMachine v3: Complete Bed Topography and Ocean Bathymetry Mapping of Greenland From

1250 Multibeam Echo Sounding Combined With Mass Conservation. *Geophys Res Lett*, 44(21), 11051-11061.

1251 doi:10.1002/2017GL074954

1252 Murphy, K. R., Stedmon, C. A., Graeber, D., & Bro, R. (2013). Fluorescence spectroscopy and multi-way

1253 techniques. *PARAFAC. Analytical Methods*, 5(23). doi:10.1039/c3ay41160e

1254 Murphy, K. R., Stedmon, C. A., Wenig, P., & Bro, R. (2014). OpenFluor– an online spectral library of auto-

1255 fluorescence by organic compounds in the environment. *Anal. Methods*, 6(3), 658-661.

1256 doi:10.1039/c3ay41935e

1257 Musilova, M., Tranter, M., Wadham, J., Telling, J., Tedstone, A., & Anesio, Alexandre M. (2017). Microbially

1258 driven export of labile organic carbon from the Greenland ice sheet. *Nature Geoscience*, 10(5), 360-365.

1259 doi:10.1038/ngeo2920

1260 Nienow, P., Sharp, M., & Willis, I. (1998). Seasonal changes in the morphology of the subglacial drainage system,

1261 Haut Glacier d'Arolla, Switzerland. *Earth Surface Processes and Landforms*, 23(9), 825-843.

1262 doi:10.1002/(sici)1096-9837(199809)23:9<825::Aid-esp893>3.0.Co;2-2

1263 Noël, B., van de Berg, W. J., Lhermitte, S., Wouters, B., Schaffer, N., & van den Broeke, M. R. (2018). Six Decades

1264 of Glacial Mass Loss in the Canadian Arctic Archipelago. *Journal of Geophysical Research: Earth*

1265 *Surface*, 123(6), 1430-1449. doi:10.1029/2017jf004304

1266 Oliver, H., Castelao, R. M., Wang, C., & Yager, P. L. (2020). Meltwater-Enhanced Nutrient Export From

1267 Greenland's Glacial Fjords: A Sensitivity Analysis. *Journal of Geophysical Research: Oceans*, 125(7).

1268 doi:10.1029/2020jc016185

1269 Östlund, H. G., & Hut, G. (1984). Arctic Ocean water mass balance from isotope data. *Journal of Geophysical*

1270 *Research*, 89(C4). doi:10.1029/JC089iC04p06373

1271 Painter, S. C., Henson, S. A., Forryan, A., Steigenberger, S., Klar, J., Stinchcombe, M. C., . . . Moore, C. M. (2014).

1272 An assessment of the vertical diffusive flux of iron and other nutrients to the surface waters of the subpolar

1273 North Atlantic Ocean. *Biogeosciences*, 11(8), 2113-2130. doi:10.5194/bg-11-2113-2014

1274 Pautler, B. G., Woods, G. C., Dubnick, A., Simpson, A. J., Sharp, M. J., Fitzsimons, S. J., & Simpson, M. J. (2012).

1275 Molecular characterization of dissolved organic matter in glacial ice: coupling natural abundance ¹H NMR

1276 and fluorescence spectroscopy. *Environ Sci Technol*, 46(7), 3753-3761. doi:10.1021/es203942y

1277 Pomeroy, L. R. (1974). The Ocean's Food Web, A Changing Paradigm. *BioScience*, 24(9), 499-504.

1278 doi:10.2307/1296885

1279 Randelhoff, A., Holding, J., Janout, M., Sejr, M. K., Babin, M., Tremblay, J.-É., & Alkire, M. B. (2020). Pan-Arctic
1280 Ocean Primary Production Constrained by Turbulent Nitrate Fluxes. *Frontiers in Marine Science*, 7.
1281 doi:10.3389/fmars.2020.00150

1282 Ravier, E., & Buoncristiani, J. (2018). Chapter 12: Glaciohydrogeology. In J. v. d. Meer & J. Menzies (Eds.), *Past*
1283 *Glacial Environments*: Elsevier.

1284 RGI Consortium (2017). Randolph Glacier Inventory – A Dataset of Global Glacier Outlines: Version 6.0:
1285 Technical Report. *Global Land Ice Measurements from Space*, Colorado, USA. Digital Media.
1286 doi:https://doi.org/10.7265/N5-RGI-60

1287 Richards, K., Sharp, M., Arnold, N., Gurnell, A., Clark, M., Tranter, M., . . . Lawson, W. (1996). An Integrated
1288 Approach to Modelling Hydrology and Water Quality in Glacierized Catchments. *Hydrological Processes*,
1289 10(4), 479-508. doi:10.1002/(sici)1099-1085(199604)10:4<479::Aid-hyp406>3.0.Co;2-d

1290 Segawa, T., Ishii, S., Ohte, N., Akiyoshi, A., Yamada, A., Maruyama, F., . . . Takeuchi, N. (2014). The nitrogen
1291 cycle in cryoconites: naturally occurring nitrification-denitrification granules on a glacier. *Environ*
1292 *Microbiol*, 16(10), 3250-3262. doi:10.1111/1462-2920.12543

1293 Sharp, M. (2005). Subglacial Drainage. In M. G. Anderson (Ed.), *Encyclopedia of Hydrological Sciences* (Vol. 167,
1294 pp. Chapter 14): John Wiley & Sons.

1295 Sharp, M., Burgess, D. O., Cogley, J. G., Ecclestone, M., Labine, C., & Wolken, G. J. (2011). Extreme melt on
1296 Canada's Arctic ice caps in the 21st century. *Geophysical Research Letters*, 38(11), n/a-n/a.
1297 doi:10.1029/2011gl047381

1298 Shepherd, A., Ivins, E., Rignot, E., Smith, B., Broeke, M. v. d., Velicogna, I., . . . Wuite, J. (2020). Mass balance of
1299 the Greenland Ice Sheet from 1992 to 2018. *Nature*, 579(7798), 233-239. doi:10.1038/s41586-019-1855-2

1300 Smith, H. J., Diesler, M., McKnight, D. M., SanClements, M. D., & Foreman, C. M. (2018). Relationship between
1301 dissolved organic matter quality and microbial community composition across polar glacial environments.
1302 *FEMS Microbiol Ecol*, 94(7). doi:10.1093/femsec/fiy090

1303 Smith, H. J., Foster, R. A., McKnight, D. M., Lisle, J. T., Littmann, S., Kuypers, M. M. M., & Foreman, C. M.
1304 (2017). Microbial formation of labile organic carbon in Antarctic glacial environments. *Nature Geoscience*,
1305 10(5), 356-359. doi:10.1038/ngeo2925

1306 Sorensen, H. L., Thamdrup, B., Jeppesen, E., Rysgaard, S., & Glud, R. N. (2017). Nutrient availability limits
1307 biological production in Arctic sea ice melt ponds. *Polar Biol*, 40(8), 1593-1606. doi:10.1007/s00300-017-
1308 2082-7

1309 St-Onge, M. R., Van Gool, J. A. M., Garde, A. A., & Scott, D. J. (2009). Correlation of Archaeal and
1310 Palaeoproterozoic units between northeastern Canada and western Greenland: constraining the pre-
1311 collisional upper plate accretionary history of the Trans-Hudson orogen. *Geological Society, London*,
1312 *Special Publications*, 318(1), 193-235. doi:10.1144/sp318.7

1313 Stedmon, C. A., & Markager, S. (2005). Resolving the variability in dissolved organic matter fluorescence in a
1314 temperate estuary and its catchment using PARAFAC analysis. *Limnology and Oceanography*, 50(2), 686-
1315 697. doi:10.4319/lo.2005.50.2.0686

1316 Stedmon, C. A., Markager, S., & Bro, R. (2003). Tracing dissolved organic matter in aquatic environments using a
1317 new approach to fluorescence spectroscopy. *Marine Chemistry*, 82(3-4), 239-254. doi:10.1016/s0304-
1318 4203(03)00072-0

1319 Stedmon, C. A., Markager, S., Tranvik, L., Kronberg, L., Slätis, T., & Martinsen, W. (2007). Photochemical
1320 production of ammonium and transformation of dissolved organic matter in the Baltic Sea. *Marine*
1321 *Chemistry*, 104(3-4), 227-240. doi:10.1016/j.marchem.2006.11.005

1322 Straneo, F., & Cenedese, C. (2015). The Dynamics of Greenland's Glacial Fjords and Their Role in Climate. *Ann*
1323 *Rev Mar Sci*, 7, 89-112. doi:10.1146/annurev-marine-010213-135133

1324 Telling, J., Stibal, M., Anesio, A. M., Tranter, M., Nias, I., Cook, J., . . . Hodson, A. (2012). Microbial nitrogen
1325 cycling on the Greenland Ice Sheet. *Biogeosciences*, 9(7), 2431-2442. doi:10.5194/bg-9-2431-2012

1326 Timmermans, M. L., & Marshall, J. (2020). Understanding Arctic Ocean Circulation: A Review of Ocean Dynamics
1327 in a Changing Climate. *Journal of Geophysical Research: Oceans*, 125(4), e2018JC014378.
1328 doi:10.1029/2018jc014378

1329 Tranter, M., Sharp, M. J., Lamb, H. R., Brown, G. H., Hubbard, B. P., & Willis, I. C. (2002). Geochemical
1330 weathering at the bed of Haut Glacier d'Arolla, Switzerland? a new model. *Hydrological Processes*, 16(5),
1331 959-993. doi:10.1002/hyp.309

1332 Tremblay, J.-É., & Gagnon, J. (2009). *The effects of irradiance and nutrient supply on the productivity of Arctic*
1333 *waters: a perspective on climate change*. Paper presented at the NATO Science for Peace and Security
1334 Series C: Environmental Security.

1335 Van Wychen, W., Burgess, D. O., Gray, L., Copland, L., Sharp, M., Dowdeswell, J. A., & Benham, T. J. (2014).
1336 Glacier velocities and dynamic ice discharge from the Queen Elizabeth Islands, Nunavut, Canada.
1337 *Geophysical Research Letters*, 41(2), 484-490. doi:10.1002/2013gl058558

1338 Van Wychen, W., Copland, L., & Burgess, D. (2020). Ice Masses of the Eastern Canadian Arctic Archipelago. In S.
1339 O. & C. N. (Eds.), *Landscapes and Landforms of Eastern Canada. World Geomorphological Landscapes*:
1340 Springer.

1341 Van Wychen, W., Copland, L., Burgess, D. O., Gray, L., Schaffer, N., & Fisher, T. (2015). Glacier velocities and
1342 dynamic discharge from the ice masses of Baffin Island and Bylot Island, Nunavut, Canada. *Canadian*
1343 *Journal of Earth Sciences*, 52(11), 980-989. doi:10.1139/cjes-2015-0087

1344 Vibe, C. (1939). Preliminary investigations on shallow water animal communities in the Upernavik- und Thule-
1345 districts (northwest Greenland). *Meddelelser om Gronland*, 124, 1-43.

1346 Vöggtli, K. (1967). D.C. Resistivity Soundings on Devon Island, N.W.T., Canada. *Journal of Glaciology*, 6(47), 635-
1347 642. doi:10.3189/s0022143000019900

1348 Wadham, J. L., Hawkings, J., Telling, J., Chandler, D., Alcock, J., O'Donnell, E., . . . Nienow, P. (2016). Sources,
1349 cycling and export of nitrogen on the Greenland Ice Sheet. *Biogeosciences*, 13(22), 6339-6352.
1350 doi:10.5194/bg-13-6339-2016

1351 Walker, S. A., Amon, R. M. W., Stedmon, C., Duan, S., & Louchouart, P. (2009). The use of PARAFAC modeling
1352 to trace terrestrial dissolved organic matter and fingerprint water masses in coastal Canadian Arctic surface
1353 waters. *Journal of Geophysical Research*, 114, G00F06. doi:10.1029/2009jg000990

1354 Whalen, J. B., Wodicka, N., Taylor, B. E., & Jackson, G. D. (2010). Cumberland batholith, Trans-Hudson Orogen,
1355 Canada: Petrogenesis and implications for Paleoproterozoic crustal and orogenic processes. *Lithos*, 117(1-
1356 4), 99-118. doi:10.1016/j.lithos.2010.02.008

1357 Wolff, E. W. (2013). Ice sheets and nitrogen. *Philos Trans R Soc Lond B Biol Sci*, 368(1621), 20130127.
1358 doi:10.1098/rstb.2013.0127

1359 Woodgate, R. A., Aagaard, K., Swift, J. H., Falkner, K. K., & Smethie, W. M. (2005). Pacific ventilation of the
1360 Arctic Ocean's lower halocline by upwelling and diapycnal mixing over the continental margin.
1361 *Geophysical Research Letters*, 32(18), L18609. doi:10.1029/2005gl023999

1362 World Glacier Monitoring, S. (2008) Global glacier changes. In. *Supplement to: World Glacier Monitoring Service*
1363 *(2008): Fluctuations of Glaciers 2000-2005. In: Haeberli, W; Zemp, M; Paul, F; Hoelzle, M (eds.), ICSU*
1364 *(FAGS) / IUGG (IACS) / UNEP / UNESCO / WMO, World Glacier Monitoring Service, Zurich,*
1365 *Switzerland, IX, 266 pp, hdl:10013/epic.39784.d001: PANGAEA.*

1366 Wyatt, F. R., & Sharp, M. J. (2017). Linking surface hydrology to flow regimes and patterns of velocity variability
1367 on Devon Ice Cap, Nunavut. *Journal of Glaciology*, 61(226), 387-399. doi:10.3189/2015JoG14J109

1368 Yamashita, Y., Fichot, C. G., Shen, Y., Jaffé, R., & Benner, R. (2015). Linkages among fluorescent dissolved
1369 organic matter, dissolved amino acids and lignin-derived phenols in a river-influenced ocean margin.
1370 *Frontiers in Marine Science*, 2(92). doi:10.3389/fmars.2015.00092

1371 Zhang, Y., Chen, C., Beardsley, R. C., Gao, G., Lai, Z., Curry, B., . . . Xu, Q. (2016). Studies of the Canadian Arctic
1372 Archipelago water transport and its relationship to basin-local forcings: Results from AO-FVCOM. *Journal*
1373 *of Geophysical Research: Oceans*, 121(6), 4392-4415. doi:10.1002/2016jc011634

1374 Zhu, Y., Suggett, D. J., Liu, C., He, J., Lin, L., Le, F., . . . Hao, Q. (2019). Primary Productivity Dynamics in the
1375 Summer Arctic Ocean Confirms Broad Regulation of the Electron Requirement for Carbon Fixation by
1376 Light-Phytoplankton Community Interaction. *Frontiers in Marine Science*, 6, 275.
1377 doi:10.3389/fmars.2019.00275

1378